Abstract

New therapeutic strategy for amyotrophic lateral sclerosis

Yasuto Itoyama

from

Department of Neurology, Tohoku University School of Medicine, 2-1 Seiryo-machi, Aoba-ku, Sendai 980-8574, Japan.

Amyotrophic lateral sclerosis (ALS) is a late onset, slowly progressive and ultimately fatal neurodegenerative disease, caused by the loss of motor neurons in the brain and spinal cord. ALS is thought to be one of the most relentless neurological diseases. The cause of ALS remains unknown, but a mutant Cu/Zn superoxide dismutase (SOD1) gene is thought to be one of most likely causes. Unfortunately, there are no effective medicines for this disease. In order to develop a new therapeutic method or medicines for ALS, we invented a new ALS rat model, SOD1 transgenic rat, which is 20 times larger in size than the mouse ALS model. Hepatocyte growth factor (HGF), which was discovered by Professor Nakamura in Osaka University, is known to have a potent neurotrophic effect on motor neurons. Our recent experimental trial in which HGF was continuously administered to ALS rats by an intrathecal route after the onset of disease showed significant effects on the clinical course and histopathological findings. ALS rats in the HGF group survived 1.6 times longer than those in the placebo group. For the clinical application of HGF for patients with ALS, we are now determining the safe doses and duration of HGF medication or possible side effects using marmosets. Additionally, genetical treatment and neural stem cell transplantation are discussed as a promising new treatment for ALS.

(*Received : September 20, 2006*)

Shinkei Kenkyu no Shinpo (Advances in Neurological Sciences), Vol. 50, No. 6, pp913-919, 2006.
IGAKU-SHOIN Ltd., Tokyo, Japan.

Behavioral/Systems/Cognitive

Separation of μ-Opioid Receptor Desensitization and Internalization: Endogenous Receptors in Primary Neuronal Cultures

Seksiri Arttamangkul,[1]* Maria Torrecilla,[1]* Kazuto Kobayashi,[2] Hideyuki Okano,[3,4] and John T. Williams[1]

[1]Vollum Institute, Oregon Health and Science University, Portland, Oregon 97239, [2]Department of Molecular Genetics, Institute of Biomedical Sciences, Fukushima Medical University, School of Medicine, Fukushima 960-1295, Japan, [3]Core Research for Evolutional Science and Technology, Japan Science and Technology Agency, Kawaguchi, Saitama 332-0012, Japan, and [4]Department of Physiology, Keio University, School of Medicine, Tokyo 160-8582, Japan

A close relationship between desensitization and internalization of μ-opioid receptors (MORs) has been proposed based on differential actions of series of agonists. The role that these two processes have in the development of tolerance and dependence to opioids has been a controversial subject that has been studied in a variety of model systems. Here, we examine desensitization and internalization of endogenous MORs simultaneously in primary cultures of locus ceruleus neurons using fluorescently tagged peptide agonists. With the use of two fluorescent opioid peptides, dermorphin-Bodipy Texas Red and dermorphin-Alexa594 (Derm-A594), desensitization was measured electrophysiologically and trafficking was followed by the accumulation of intracellular fluorescent puncta. Blocking endocytosis with concanavalin A eliminated the accumulation of fluorescent puncta but desensitization induced by Derm-A594 was unaffected. Likewise, after treatment with concanavalin A, there was no change in either desensitization or recovery from desensitization induced by [Met]^{5}enkephalin. The results demonstrate that desensitization and the recovery from desensitization are not dependent on receptor internalization and suggest that the activity of endogenous MORs in primary neurons can be modulated at the level of the plasma membrane.

Key words: fluorescent-peptide; locus ceruleus; culture; concanavalin A; electrophysiology; two-photon microscopy

Introduction

The activation of μ-opioid receptors (MORs) mediates the analgesic effects of opioids and repeated activation of these receptors results in tolerance so that a higher concentration of opioids are required to achieve the same level of analgesia (Contet et al., 2004). Two early events that follow the activation of MORs are the development of acute desensitization and induction of receptor trafficking (Ferguson, 2001; Connor et al., 2004; Bailey and Connor, 2005). With the use of a series of agonists, it was determined that agonists that cause desensitization also promote receptor trafficking, an observation that has been taken to suggest that the two processes are closely linked (Keith et al., 1996; Alvarez et al., 2002; von Zastrow et al., 2003). Morphine in particular was an agonist that did not cause desensitization or internalization. These results led to the hypothesis that receptor internalization was a mechanism that prevented adaptive changes that initiate the development of tolerance (Whistler et al., 1999; Finn and Whistler, 2001). Recent work has indicated that, although morphine may not be as efficient as other agonists, it can cause both desensitization (Borgland et al., 2003; Dang and Williams, 2005; Koch et al., 2005) and internalization (Haberstock-Debic et al., 2005). The discrepancy between studies has led to an alternate hypothesis suggesting that internalization plays an important role in the recovery from desensitization (Koch et al., 2005). This alternate hypothesis proposes that internalization is the primary mechanism whereby receptors can be removed from the desensitized state. Because morphine does not cause efficient trafficking it results in much more desensitization than other agonists (Koch et al., 2005). The conflicting theories may well result from marked difference in the experimental models (Connor et al., 2004; Bailey and Connor, 2005). Most studies have used systems in which receptors are overexpressed and that measured both internalization and desensitization in separate experiments with different experimental protocols. Very little work has been done in primary neurons looking at endogenously expressed receptors.

One limitation of using native neurons to study receptor trafficking is difficulty in following the endogenous receptor in real time. Fluorescent opioid ligands have been used successfully to follow receptor internalization in Chinese hamster ovary and human embryonic kidney 293 (HEK293) cells expressing cloned

Received Nov. 18, 2005; revised March 1, 2006; accepted March 2, 2006.

This work was supported by National Institutes of Health Grants DA016627 (S.A.) and DA08163 (M.T., J.T.W.) and by the National Alliance for Research on Schizophrenia and Depression (J.T.W.). M.T. was also supported in part by a postdoctoral fellowship from the Basque Government. We thank Charles Jimenez for producing the fluorescent peptides. We thank Drs. Shane Hentges and Susan Ingram for their advice for primary culture techniques and Heather Dought and Terri Vermillion for animal care. We are also grateful to Dr. Susan Amara for the use of the confocal microscope.

*S.A. and M.T. contributed equally to this work.

Correspondence should be addressed to John T. Williams, Vollum Institute, Oregon Health and Science University, 3181 Southwest Sam Jackson Park Road, Portland, OR 97239. E-mail: williamj@ohsu.edu.

DOI:10.1523/JNEUROSCI.0303-06.2006

 0270-6474/06/264118-08$15.00/0

MORs (Arttamangkul et al., 2000; Alvarez et al., 2002) as well as rat cortical neurons in cultures (Lee et al., 2002). In this study, fluorescent peptides were used to study MOR activation, desensitization, and internalization in primary neuronal cultures from the mouse locus ceruleus (LC). The LC neurons were identified by the presence of green fluorescent protein (GFP) that was expressed under the tyrosine hydroxylase promoter (TH-EGFP) (Sawamoto et al., 2001; Matsushita et al., 2002). Cultured LC neurons had functional MORs as determined by activation of G-protein-activated inwardly rectified potassium channels (GIRKs), inhibition of voltage-dependent calcium channels, and inhibition of synaptic transmitter release at recurrent synapses (autapses). Both desensitization and internalization were studied on the same cell and the results showed that receptor desensitization and recovery from desensitization were not changed after internalization was blocked with concanavalin A (con A).

Materials and Methods

Cultures. The TH-EGFP mice generated in Dr. Kobayashi's laboratory (Sawamoto et al., 2001) were backcrossed to DBA-2J for at least five generations before these experiments. Only heterozygous animals were used because homozygous mice did not survive for more than a few weeks. Mice (3–5 weeks) were used for these experiments to ensure that the brains were fully developed before the cultures were made. The care and use of animals were conducted in accordance with the National Institutes of Health guidelines and with an approval from the Institutional Animal Care and Use Committee of the Oregon Health and Science University. Animals were anesthetized with halothane and decapitated. The brain was removed and sliced horizontally using a vibratome (Leica, Nussloch, Germany) in ice-cold artificial CSF (ACSF) containing the following (in mM): 126 NaCl, 2.5 KCl, 1.2 $MgCl_2$, 1.2 NaH_2PO_4, 2.4 $CaCl_2$, 21.4 $NaHCO_3$, and 11 glucose. Slices were equilibrated in warm (35°C) oxygenated ACSF solution for 15 min and the area around the LC was microdissected with two 23-gauge needles under a dissecting microscope. The tissues were incubated in dissociation buffer containing papain (20 U/ml; Worthington Biochemical, Lakewood, NJ) for 5–7 min. The dissociation buffer, adjusted to pH 7.4, contained the following (in mM): 81.8 Na_2SO_4, 30 K_2SO_4, 12 $MgCl_2$, 0.25 $CaCl_2$, 4 HEPES, 0.2 glucose, and phenol red. Dissociation was done in the growing media containing Neurobasal A, 2% heat-inactivated fetal bovine serum (FBS), 1 mM glutamine, B-27 nutrient mix (all from Invitrogen, San Diego, CA), and 0.5 mM kynurenate (Sigma, St. Louis, MO) by trituration with a series of pasture pipettes having decreasing tip sizes. The cell suspension was plated onto glial feeder previously grown on glass coverslips. A glial feeder layer was prepared from the neonatal cortex and was allowed to grow until a monolayer formed. The media for glial cells contained MEM (Invitrogen), 0.1% mitogenic serum extender (BD Biosciences), 30 mM glucose, and 4% non-heat-inactivated fetal calf serum. After LC neurons were plated onto the feeder layer, media were changed from 2 to 1% FBS of growing media on the next day and then a complete serum-free media (Neurobasal A, 1 mM glutamine, B-27, and 0.5 mM kynurenate) for the following feeding schedule. The cultures were grown in the serum-free media for at least 5 d before being used in the experiments.

Whole-cell recording. Coverslips containing the LC neurons were transferred to a recording chamber and perfused with ACSF solution equilibrated with 95% O_2 and 5% CO_2 to pH 7.4. Noradrenergic neurons were identified as large green fluorescent cells using a Zeiss (Oberkochen, Germany) Axioskop 2 FS fluorescent microscope. Recordings were made with patch pipettes (2 MΩ) containing the following (in mM): 115 potassium gluconate, 20 NaCl, 1.5 $MgCl_2$, 0.1 EGTA, 5 HEPES, 2 Mg-ATP, 0.5 Na-GTP, and 10 phosphocreatine, pH 7.4 (280 mOsm/kg). To record inward potassium currents, the membrane potential was hyperpolarized from −60 to −100 mV for 30 ms in a high-potassium (10 mM) solution at room temperature (25°C). To record the Ca^{2+}/Ba^{+} inward currents, CsCl was substituted for potassium gluconate and the external solution contained $BaCl_2$ (1 mM) and tetrodotoxin (300 nM; Alomone Laboratories, Jerusalem, Israel). To study the release of transmitter from cultured LC neurons, autaptic currents were evoked by depolarizing the membrane potential −60 to −20 mV for 2 ms. All drugs and solutions were perfused onto the cultures by gravity flow or a fast-flow valve system (Warner Instrument, Hamden, CT). The peptidase inhibitors bestatin (10 μM) and thiorphan (2 μM) were included in all solutions containing opioid peptides to prevent peptide metabolism (Williams et al., 1987). [Met]^{5}enkephalin (ME), thiorphan, and bestatin were obtained from Sigma. 5-Bromo-*N*-[4,5-dihydro-1*H*-imidazol-2-yl]-6-quinoxalinamine (UK14304) was obtained from Research Biochemical (Natick, MA). Dermorphin-Bodipy Texas Red (Derm-BTR) and dermorphin-Alexa594 (Derm-A594) were prepared as described in Arttamangkul et al. (2000). Morphine was obtained from the National Institute of Drug Abuse. 3-Dioxobenzo[f]quinoxaline-7-sulfonamide (NBQX) was obtained from Tocris (Ellisville, MO). Whole-cell recordings were made with an Axopatch-1D (Molecular Devices, Union City, CA), filtered at 5 kHz, and digitized with an ITC-16 computer interface (Instrutech, Long Island, NY). Data were sampled at 10 kHz with Axograph 4.5 software. The membrane potential was held at −60 mV. All patch-clamp experiments were done at room temperature. Data are presented as means ± SEM. All statistical comparisons were made using Student's *t* test and the level of significance was considered as $p < 0.05$.

Confocal microscopy. Neurons were submerged in serum-free media plus HEPES buffer (50 mM). Derm-BTR solution containing bestatin (10 μM) and thiorphan (2 μM) was added to the cells with the temperature of the chamber set at 15°C. Images were captured at various times after the temperature was rapidly raised (within 1 min) to 35°C. Images were acquired on a Bio-Rad (Hercules, CA) MRC-1024 confocal microscope equipped with a krypton–argon laser. Cells were visualized under a Plan Apo 60× (1.4 numerical aperture, oil) objective lens. The filters used for scanning green fluorescent protein were 488 (excitation) and 522 nm (emission), and for Derm-BTR they were 568 (excitation) and 585 nm (emission). Acquisition parameters were averaged two frames per image using a direct filter to prevent photobleaching and normal scanning mode. All images were processed using CAS 40 software (Bio-Rad), ImageJ (National Institutes of Health, Bethesda, MD), and Adobe (San Jose, CA) Photoshop 6.0.

Two-photon microscopy and intracellular recording. Simultaneous recording of membrane potential and imaging was done with an electrophysiological setup equipped with a custom-built two-photon microscope. Intracellular recordings of membrane potential were done with glass electrodes filled with KCl (300 mM) having a resistance of 100–200 MΩ. Experiments with a combination of intracellular recordings and imaging were all done at 35°C. Data collection was done with Power Lab (Chart version 4.1). Drugs were applied by perfusion. Images were acquired using Scan Image software (Pologruto et al., 2003). The Ti-sapphire laser was set at 810 nm. The emission filter sets were 510 nm for EGFP and 600 nm for Derm-A594. Cells were imaged with a z-series taken through the cell at 0.5 μm intervals, averaging two frames per image. Data were processed off-line using Image J and Adobe Photoshop 6.0.

Results

Cultured LC neurons

The LC is a dense and compact group of green fluorescent neurons located on the lateral aspect of the fourth ventricle in slices from the TH-EGFP mice (Fig. 1*A*,*B*). The GFP fluorescent cells costained with anti-tyrosine hydroxylase antibodies, thus confirming that they were noradrenergic (Fig. 1*C*). Cultures were prepared from animals that were 3–5 weeks old and used within 14 d of plating. Generally, there were approximately five GFP-positive neurons per coverslip. Some cells were isolated having no contact with other neurons (Fig. 1*D*). LC neurons were identified by the presence of GFP and the characteristic morphology when viewed with infrared illumination. Cells were large (>20 μm) with a round cell body and multipolar processes and exhibited dark granulated vesicles. ~90% of cells having these characteristic responded robustly to the α_2-adrenergic agonist UK14304 and of those cells a small percentage (~25%) were equally sensitive to

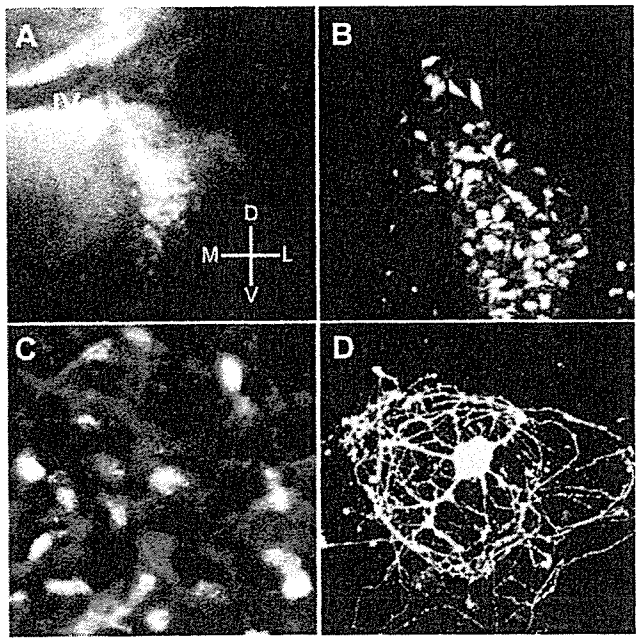

Figure 1. LC neurons expressing GFP. ***A***, The LC is found next to the fourth ventricle (10×). ***B***, An enlarged image showing the dense and compact structure of the nucleus (20×). ***C***, Colocalization of GFP and anti-tyrosine hydroxylase (mouse monoclonal) labeled with Texas Red-conjugated secondary antibody. ***D***, A single neuron in culture for 9 d.

opioid agonists. The reason that many cells responded poorly to opioids is not clear, but was dependent on the culture. Only cells that responded robustly to ME were included in this study.

Opioid actions

Opioids are known to have three different actions on LC neurons, an increase in potassium conductance, an inhibition of voltage-dependent calcium current, and an inhibition of noradrenaline release from terminal regions (Williams et al., 2001). In the present study, each of these actions was studied. As has been observed in slice and acutely dissociated cell preparations, opioid agonists increased GIRK conductance in cultured neurons (Fig. 2*A*). Experiments were done in a high-potassium (10 mM) solution to increase the amplitude of the GIRK current. Cells were held at −60 mV, stepped to −100 mV, and the inward potassium current measured at −100 mV. ME, morphine, Derm-BTR, and an α_2-adrenergic agonist UK14304 increased potassium currents. To make comparisons between cells, the currents induced by different opioid agonists were normalized to the current produced by UK14304 (10 μM). The amplitude of the ME (30 μM) (Fig. 2*A*) current was similar to that induced by UK14304, having a ratio of 0.91 ± 0.07 (n = 12). Morphine (10 μM) induced a current that was approximately one-half the size of that induced by UK14304 (ratio = 0.45 ± 0.04; n = 5). The results suggested that morphine was a weak agonist at MOR in these cultured neurons. The fluorescent peptide agonist Derm-BTR was tested at two different concentrations (0.1 and 1 μM). Both applications produced potassium currents that were about one-half of current induced by UK14304 (Derm-BTR, 0.1 μM = 0.54 ± 0.12, n = 3; Derm-BTR, 1 μM = 0.56 ± 0.08, n = 8) (Fig. 2*A*). This finding agreed with previous work done in rat brain slices indicating that Derm-BTR was less efficacious than ME (Arttamangkul et al., 2000).

Opioids have been demonstrated to inhibit calcium (barium) currents in dissociated LC neurons and slices (Ingram et al., 1997; Chieng and Bekkers, 1999; Connor et al., 1999: Torrecilla et al., 2002). The membrane potential was depolarized from −60 to −20 mV for 10 ms to activate an inward current carried by calcium and barium. ME (30 μM) and Derm-BTR (0.1 μM) decreased barium currents by 27.5 ± 3.6% (n = 9) and 26.4 ± 1.6% (n = 3), respectively (Fig. 2*B*). Unlike activation of GIRKs, Derm-BTR produced the same maximal inhibition as ME. As was suggested in experiments done in acutely dissociated LC neurons, it appears that the coupling of opioid receptors to the inhibition of calcium (barium) currents is more efficient than that required to activate potassium currents (Ingram et al., 1997). The activation of α_2-adrenergic receptors by UK14304 also reduced the inward calcium (barium) current by 45.8 ± 2.1% (n = 3).

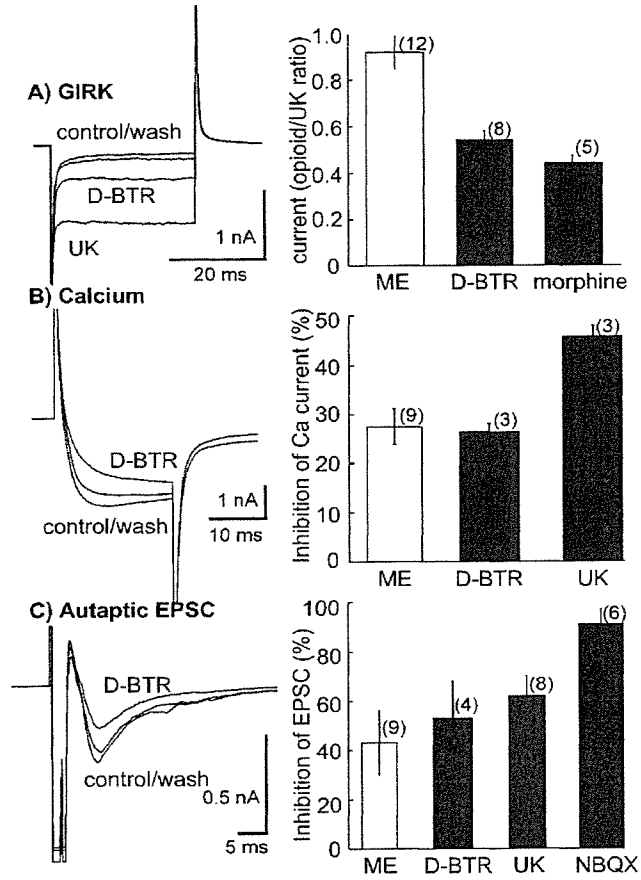

Figure 2. Effectors sensitive to the activation of MORs. ***A***, Activation of GIRK conductance. Whole-cell recordings were made in a high-potassium (10 mM) solution (V-hold −60 mV, step to −100 mV). Inward currents were measured at −100 mV. The superimposed traces show the currents triggered by Derm-BTR (D-BTR; 1 μM) and UK14304 (UK; 10 μM). The bar graph summarizes the currents induced by opioid agonists normalized to the current induced by UK14304. Both Derm-BTR (1 μM) and morphine (10 μM) were partial agonists in this assay. ***B***, Inhibition of voltage-dependent calcium (barium) conductance. Whole-cell recordings were made and the inward current induced by a depolarizing step from −60 to −20 mV was measured. Representative traces show the inhibition caused by Derm-BTR (0.1 μM). The bar graph summarizes the inhibition of calcium (barium) currents as percentage of control. Derm-BTR caused the same maximal inhibition as ME (30 μM) in this assay. ***C***, Recurrent synapses (autapses) mediated by glutamate are inhibited by opioids. The superimposed traces show the current induced during depolarization of cells from −60 to −10 mV followed by an EPSC. The EPSCs were inhibition by Derm-BTR (1 μM). The bar graph summarizes the inhibition of EPSCs by ME (10 μM), Derm-BTR (1 μM), UK 14304 (10 μM), and NBQX, an AMPA antagonist (10 μM). The results indicate that LC cells release glutamate when maintained in an isolated cell culture and opioids inhibit that release. Error bars indicate SE.

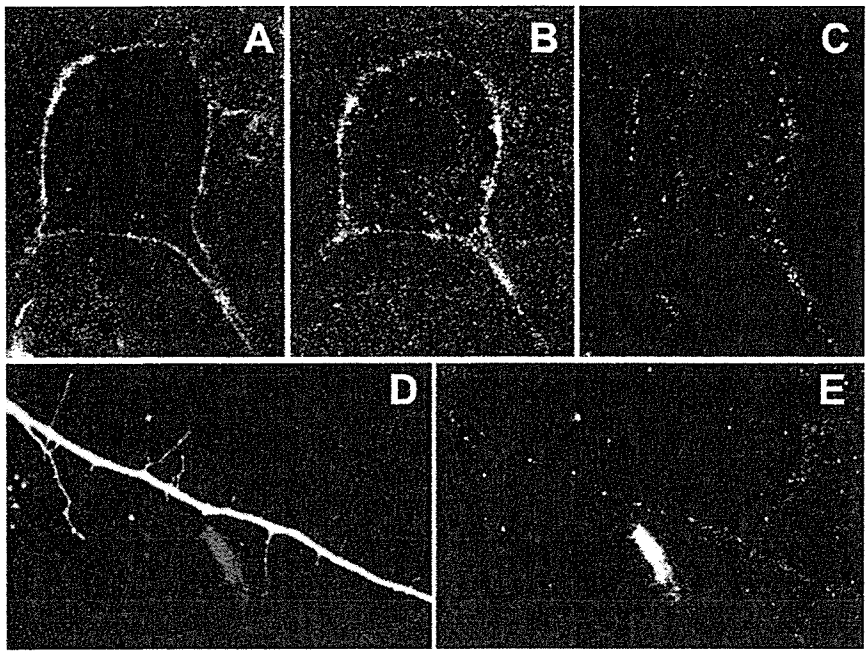

Figure 3. Internalization of Derm-BTR (450 nM). ***A***, Binding of Derm-BTR (450 nM) to receptors on the plasma membrane was observed as a fluorescent ring along plasma membrane (15°C). The temperature was then increased to 35°C within 1 min and internalization was monitored for 45 min. ***B***, Image of the same cell taken after incubation for 30 min. ***C***, After washing the Derm-BTR with a hypertonic acid solution (0.5 M NaCl in acetate buffer, pH 4), extracellular fluorescence outside the cell was removed and fluorescent puncta were observed in the soma. ***D***, ***E***, Fluorescent puncta containing Derm-BTR found in a GFP-positive process.

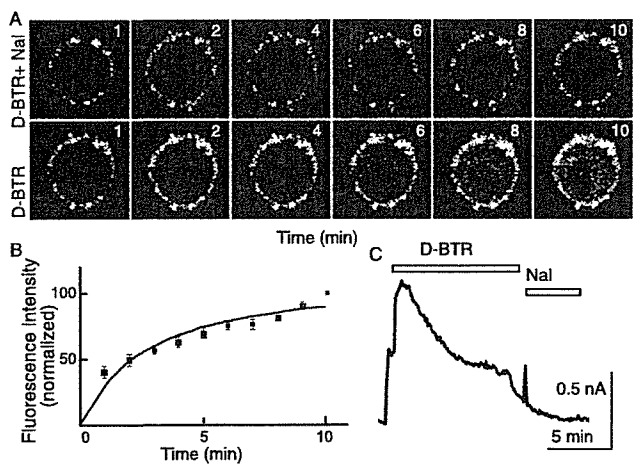

Figure 4. Time course of Derm-BTR internalization and desensitization. ***A***, A representative experiment showing the block of Derm-BTR (D-BTR; 100 nM) internalization by naloxone (10 μM; top row). Naloxone was washed from the bath and Derm-BTR (100 nM) was reapplied to demonstrate the presence of MORs on this cell. Images were taken with a confocal microscope at 2 min intervals. To reduce photobleaching, a single frame was collected at each of 5 z-planes. Only nonspecific staining was found in the presence of naloxone. ***B***, Fluorescent intensity in the cytoplasm increased over the first 4–5 min and reached a plateau at 10 min. The fluorescence was normalized to the intensity measured at 10 min. ***C***, A representative experiment showing the peak and decline of the potassium current induced by Derm-BTR (1 μM) during a 10 min application. The experiment was done in a high-potassium solution as in Figure 2*A*. The inward current was measured during a voltage step from −60 to −100 mV applied once every 20 s. The current is plotted as an outward current to better illustrate the decline in the current. Error bars indicate SE.

Inhibition of transmitter release is a well known action of opioids (Williams et al., 2001). Cultured LC neurons plated at low density often formed recurrent synapses (autapses) (Fig. 2*C*). When these cells were depolarized from −60 to −20 mV for 2 ms, a sharp-rising inward current was observed. The currents had a mean amplitude of 2.1 ± 0.6 nA ($n = 13$). The mean duration was ~10 ms. This EPSC was blocked by the AMPA receptor antagonist, NBQX (10 μM; 91 ± 6.2% inhibition of the control EPSC; $n = 6$). This result suggests that LC neurons, like other monoaminergic neurons (Johnson, 1994; Sulzer et al., 1998), release glutamate when maintained in isolated cell culture. Both opioids and UK14304 decreased the amplitude of the autaptic EPSC. There was no significant difference between the inhibition caused by the opioid or α_2-adrenoceptor agonists [Derm-BTR, 1 μM, 53 ± 15% inhibition ($n = 4$); ME, 10 μM, 43 ± 13% inhibition ($n = 4$); UK14304, 10 μM, 62 ± 8% inhibition ($n = 8$)].

Agonist-induced internalization

The internalization of Derm-BTR in the LC cultures was examined using a confocal microscope. As was found in experiments done with cell lines expressing Flag-tagged MORs (Arttamangkul et al., 2000; Alvarez et al., 2002), Derm-BTR resulted in the appearance of fluorescent puncta in the LC cultured neurons and was taken as a measure of receptor internalization. This internalization was opioid-receptor dependent because no fluorescent puncta were observed in the presence of naloxone (10 μM; $n = 4$). Internalization was temperature dependent. When the cell was incubated with Derm-BTR at 15°C, fluorescence was found only at the plasma membrane (Fig. 3*A*). Cells were incubated in Derm-BTR (450 nM) for a total of 45 min at 35°C. Fluorescent puncta were found in the cytoplasm primarily in the perinuclear region (Fig. 3*B*). High-resolution images of the internalized Derm-BTR were taken after a hypertonic acid wash. Fluorescent puncta were found in soma, proximal, and distal dendrites (Fig. 3*C–E*).

To determine the time course of internalization, images were taken at 2 min intervals for 10 min (Fig. 4*A*). To make comparisons between experiments, intracellular fluorescence was measured at each time point and plotted as a ratio of fluorescence measured at the end of the 10 min incubation. The fluorescence increased quickly (2–4 min) and reached a plateau within 10 min (Fig. 4*B*) ($n = 6$). The time course of internalization of Derm-BTR in the cultured LC neurons was similar to that measured in HEK cells (Alvarez et al., 2002).

Desensitization and internalization

When recordings were made during the application of Derm-BTR (1 μM, at 25°C) the potassium current rose to an initial peak and declined in the continued presence of the drug. After 10 min, the current declined to 82 ± 12% of the initial peak (Fig. 4*C*) ($n = 4$). Because Derm-BTR is a very hydrophobic molecule, it was not possible to completely wash the high concentration of Derm-BTR, particularly after a prolonged application period. Naloxone (1 μM) was used to rapidly reverse the current induced by Derm-BTR, to make an accurate measurement of the desensitization (Fig. 4*C*). Without using a hypertonic acid wash, the continued presence of extracellular fluorescent resulted in images of poor quality. It was therefore not possible to examine both desensitization and internalization in the same experiment.

Two changes in the experimental protocol were necessary to carry out experiments where desensitization and internalization could be examined on the same cell. First, intracellular recordings were used for these experiments because these recordings were stable over 60 min and did not disrupt cell morphology. High-resistance pipettes (100–200 MΩ) were used and membrane potential was measured. All experiments with intracellular recordings in combination with imaging were done at 35°C. As a control, each cell was tested with ME before imaging experiments. The amplitude of the hyperpolarization induced by ME (10 μM) was 16.1 ± 1.3 mV (n = 23), which was similar, but somewhat smaller (5–10 mV) than that measured with intracellular recordings in mouse brain-slice experiments (S. Arttamangkul, unpublished observations). The second change in the experimental protocol required the synthesis of a more hydrophilic fluorescent dermorphin analog, Derm-A594. The advantage of this compound was the increased water solubility, enabling a more rapid (5 min) and complete wash-out, even with the use of high concentrations and prolonged exposures.

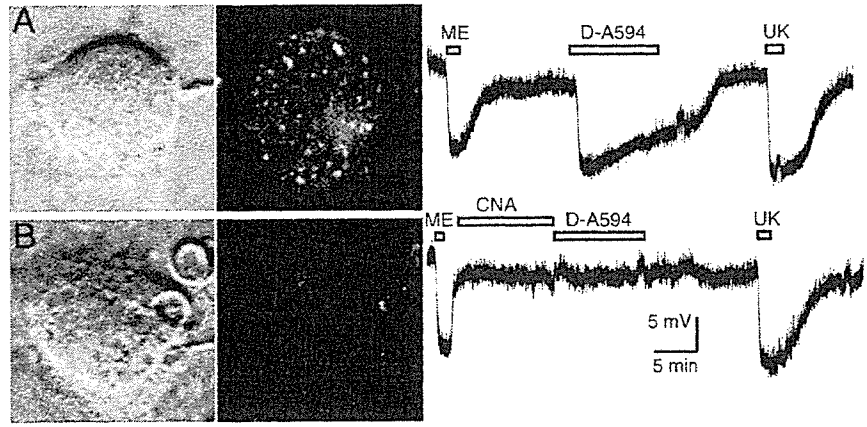

Figure 5. Desensitization and internalization in the same neuron. ***A***, Intracellular recording and two-photon microscopy were done simultaneously during treatment with Derm-A594 (D-A594). The top left shows an image of a neuron take with infrared illumination and the same neuron after incubation with Derm-A594 (6 μM, 10 min, 5 min wash; right). The trace to the right is the recording of the membrane potential of that neuron. ME (10 μM) and Derm-A594 hyperpolarized this neuron. The hyperpolarization induced by Derm-A594 peaked and declined during a 10 min application. After washing Derm-A594, UK14304 caused a maximal hyperpolarization. ***B***, The blockade of the hyperpolarization and internalization by β-CNA (1 μM).

Superfusion with Derm-A594 (6 μM) caused a hyperpolarization of 14.8 ± 2.6 mV (n = 7), not significantly different from that induced by ME (10 μM; Student's t test, p = 0.61) (Fig. 7*C*). During a 10 min application of Derm-A594 (6 μM), the peak hyperpolarization declined by 44 ± 7% (n = 5). This decline was taken as a sign of desensitization. After washing for 5 min, fluorescent puncta were present in the cytoplasm (Fig. 5, top panel). To confirm that the hyperpolarization and internalization were dependent on opioid receptors, experiments were done aftertreatment with the irreversible opioid antagonist, β-chlornaltrexamine (β-CNA; 1 μM). After β-CNA, Derm-594 (6 μM) did not change the resting membrane hyperpolarization and no fluorescent puncta were found in the neurons observed (Fig. 5, bottom panel) (n = 3).

With the combination of these measures it was possible to determine the role of receptor internalization on the desensitization process. First, the hyperpolarization induced by ME (300 nM; 12.8 ± 1.1 mV; n = 14) was tested before and after a 2 min application of Derm-A594 (6 μM) (Fig. 6). The hyperpolarization induced by ME (300 nM) tested 5 min after the application of Derm-A594 was 42 ± 5% (n = 5) of control. Thus, as was found with a 2 min application of ME in brain-slice experiments (Dang and Williams, 2004), Derm-A594 caused significant desensitization. After this short application of Derm-A594, no significant fluorescent puncta were detected (Fig. 6*B*). This may indicate that desensitization was induced in the absence of internalization. It is also possible that the intracellular fluorescence was below the limit of detection. To determine whether desensitization and internalization were separate processes, receptor desensitization was examined under conditions where internalization was blocked.

The application of concanavalin A to block receptor internalization via clathrin-dependent pathways has been shown previously (Xiang et al., 2002; Kim et al., 2004). In the present experiments, all cells were initially tested with ME (10 μM, 2 min). Concanavalin A (160 or 200 μg/ml) was superfused for 20 min

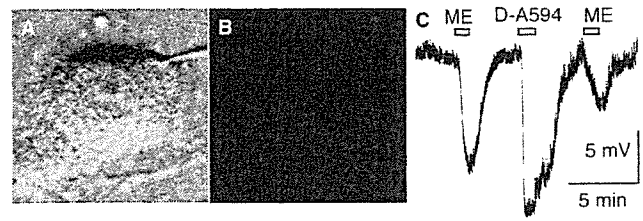

Figure 6. Desensitization by a short pulse of Derm-A594. ***A***, Image of a representative cell where desensitization resulting from a short application of Derm-A594 was measured. ***B***, Fluorescence image taken with a two-photon microscope showing the lack of any puncta after a 2 min treatment with Derm-A594 (6 μM). ***C***, Recording of membrane potential from the neuron shown in ***A*** and ***B***. Desensitization was determined by comparing the decrease in the amplitude of the hyperpolarization induced by ME (300 nM), before and after a short pulse (2 min) of Derm-A594 (D-A594; 6 μM).

followed by treatment with Derm-A594 (6 μM, in con A) for 10 min. The initial hyperpolarization induced by Derm-A594 was 15.1 ± 1.1 mV (n = 6), which declined by 45 ± 4% over the 10 min application period (n = 6) (Fig. 7). After treatment with concanavalin A, neither the peak nor the decline in the hyperpolarization induced by Derm-A594 was significantly different from control (Student's t test, p = 0.68 and p = 0.88, respectively). The block of internalization was confirmed because no fluorescent puncta were found in the cytoplasm of cells (Fig. 7, supplemental Fig. 1, available at www.jneurosci.org as supplemental material). Thus, concanavalin A blocked internalization but did not change the desensitization induced by Derm-A594, nor was the peak hyperpolarization induced by UK14304 changed (control 19.6 ± 3.6 mV; con A 16.3 ± 1.4 mV; p = 0.31) (Fig. 7).

Recovery from desensitization

The recovery from desensitization was determined by comparing the hyperpolarization induced by ME (300 nM, 2 min) before and after application of a saturating concentration of Derm-A594 (6 μM, 2 min) or ME (10 μM, 2 and 5 min). The hyperpolarization induced by ME (300 nM) was 42 ± 5 and 61 ± 6% of control 5 and 20 min after washout of Derm-A594, respectively (6 μM, 2 min; n = 5). After desensitization with ME (10 μM, 2 min), the hyperpolarization caused by ME (300 nM) was 42 ± 14 and 81 ± 12%

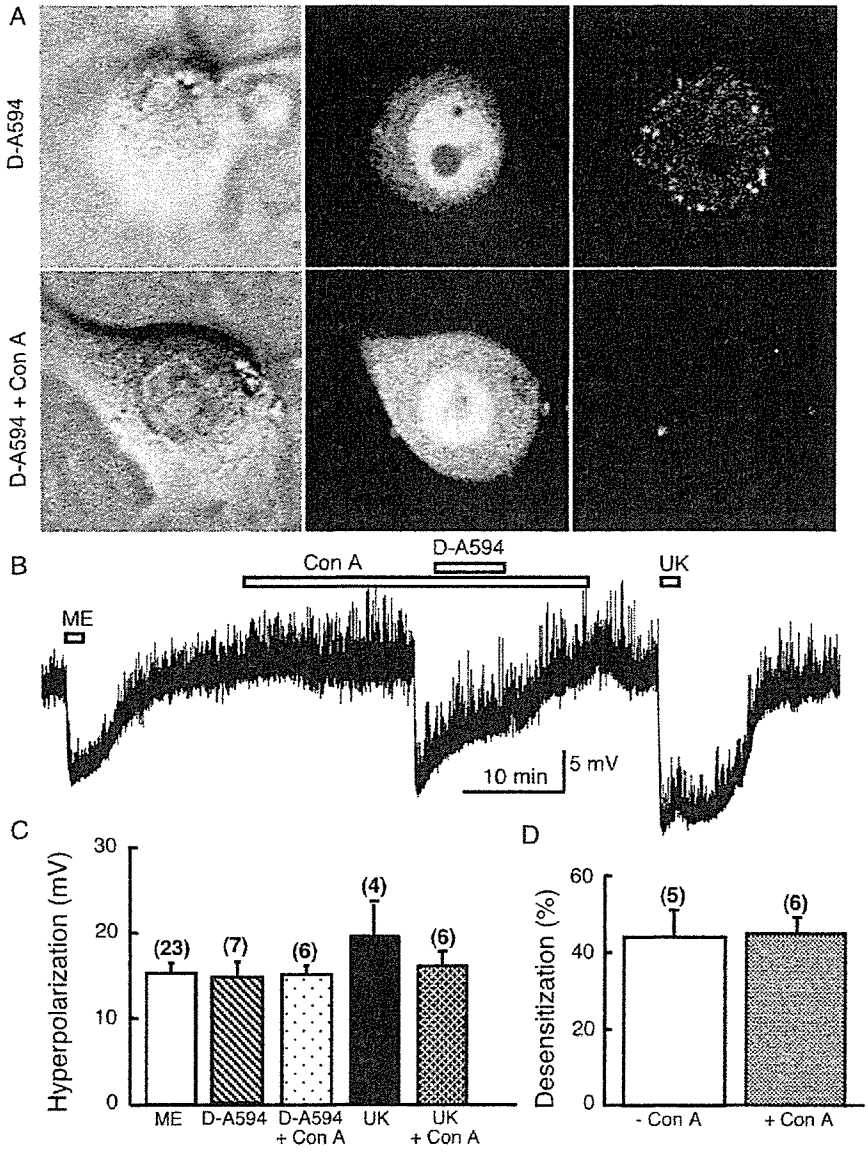

Figure 7. MOR desensitization is not changed after blockade of internalization. ***A***, Images of a neuron showing the appearance of fluorescent puncta in a control experiment (top). ***B***, Images of cell after treatment with con A. No fluorescent puncta were found. ***C***, Recording of membrane potential from a cell treated with con A. All cells were initially tested with ME (10 μM). Con A (160–200 μg/ml) was superfused for 20 min. Derm-A594 (D-A594; 6 μM, in con A) induced membrane hyperpolarization similar in amplitude to that of ME. ***D***, Summarized data showing the amplitude of the hyperpolarization induced by Derm-A594 and UK14304 (UK) in the absence and presence of con A. ***E***, shows that the decline of the hyperpolarization induced by Derm-A594 was the same in the absence and presence of con A. Error bars indicate SE.

of control after 5 and 20 min, respectively ($n = 3$) (Fig. 8*C*). The recovery from desensitization was not significantly different after washout of Derm-A594 or ME ($p = 0.14$) and was similar in time course to that found in rat brain-slice experiments (Dang and Williams, 2004).

Recovery from desensitization was next examined 5 and 20 min after the application of ME (10 μM, 5 min) in the absence and presence of concanavalin A (160 μg/ml, 20 min preincubation) (Fig. 8*A*,*B*). The hyperpolarization induced by ME (300 nM) 5 and 20 min after desensitization with ME (10 μM, 5 min) was 35 ± 8 and 70 ± 7% ($n = 4$) of control in the absence of concanavalin A and 40 ± 12 and 65 ± 10% ($n = 4$) of control in the presence of concanavalin A, respectively. There was no significant difference in the amount of recovery at either time point ($p = 0.71$ after 5 min; $p = 0.66$ after 20 min). The recovery from desensitization was therefore not changed under conditions where internalization was blocked.

Discussion

The results from this study demonstrate functional regulation of MORs in cultured LC neurons from TH-EGFP mice. With the combination of electrophysiological recording and the imaging of fluorescent opioid ligands, both desensitization and internalization were examined on the same cell under identical conditions. The use of primary cultures of neurons and fluorescent agonists made it feasible to study endogenous MORs. The results show that desensitization and the recovery from desensitization were not affected under conditions where internalization was blocked.

Effectors and receptor coupling

The results of the present study indicate that the coupling efficiency between various agonists and effectors can be distinguished. Although Derm-BTR was effective at inducing internalization, and caused a maximal inhibition of voltage-dependent calcium currents and transmitter release, it was not potent at activating GIRKs. By examining the relative action of Derm-BTR and ME on several different effectors on the same cells, it was clear that the activation of GIRKs required the more potent agonists to reach a maximal effect. This difference in agonist/receptor coupling has been observed previously in acutely dissociated LC neurons, where ME was a potent agonist at activating GIRK conductance, but morphine was an antagonist (Ingram et al., 1997). Unlike the activation of GIRK conductance, however, morphine caused an inhibition of calcium currents in acutely dissociated LC neurons (Connor et al., 1999). The coupling efficiency between MORs and the activation of GIRKs suggests that the receptor reserve was limited in this culture assay, thereby decreasing the proportion of neurons that responded to opioids. Similar results were reported in dissociated cell cultures of rat LC cells, where <50% of cells were hyperpolarized by even high concentrations of [D-Ala^2, D-Leu^5]enkephalin (DADLE; 10–30 μM) (Masuko et al., 1986). In brain-slice experiments on LC neurons, DADLE was a potent agonist that hyperpolarized all neurons through an activation of MORs (Williams and North, 1984). In the present study, each cell was tested with an EC_{50} concentration of ME (300 nM); only cells that were hyperpolarized by at least 10 mV were selected for further study. The hyperpolarization in these "healthy" cells was similar to that measured in brain-slice recordings, suggesting that the opioid receptor regulation in these neurons was not dramatically changed. Each cell also served as its own control in all

desensitization and recovery experiments. The decline in the hyperpolarization induced by the test application of ME (300 nM) after treatment with a saturating concentration of agonist was a sensitive measure to detect desensitization. Neither the extent nor the time course of recovery from desensitization was different from what has been measured in rat brain-slice experiments (Dang and Williams, 2004).

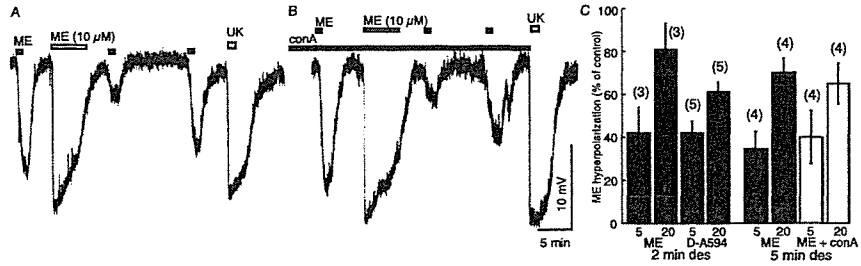

Figure 8. MOR recovery from desensitization is independent of internalization. ***A***, A representative trace showing the recovery from desensitization induced by ME (10 μM). ME (300 nM) was tested before and 5 and 20 min after application of ME (10 μM, 5 min). The α_2-adrenoceptor agonist UK14304 (1 μM) was applied at the end of the experiment. ***B***, The recovery from desensitization induced by ME (10 μM) was not changed after treatment with concanavalin A (160 μg/ml, preincubated for 20 min). ***C***, Summarized data showing the recovery from desensitization. Left, A short (2 min) application of ME (10 μM; gray bars) and Derm-A594 (D-A594; 6 μM; black bars) decreased the hyperpolarization induced by ME (300 nM) to ~40% of control 5 min after washout. After 20 min, significant recovery was observed. Right, ME (10 μM) was perfused for 5 min and the hyperpolarization induced by ME (300 nM) was tested after 5 and 20 min. The time course or extent of recovery was not changed by concanavalin A (white bars) compared with controls (gray bars). Error bars indicate SE.

Homologous desensitization

Homologous MOR desensitization has been reported in several different preparations (Kovoor et al., 1998; Borgland et al., 2003; Celver et al., 2004). In the present study, the hyperpolarization induced by an α_2-adrenoceptor agonist was not reduced after MOR desensitization. Similar results have been reported in LC cells recorded in rat brain slices (Bailey et al., 2004; Dang and Williams, 2004) (but see Blanchet and Luscher, 2002). The simplest interpretation of the present results is that a 2–10 min application of an opioid agonist induced homologous desensitization at the receptor. It is possible, however, that desensitization results from a point beyond the receptor but not at the potassium channel. One possibility would be a depletion of G-proteins that are selectively activated by opioid receptors.

Desensitization and receptor trafficking

The mechanism underlying desensitization in LC neurons remains unclear but presumably involves receptor phosphorylation by G-protein-receptor kinases and translocation of β-arrestin (Gainetdinov et al., 2004). This sequence could result in a blockade of signaling without internalization, however, the binding of arrestin to the ligand/receptor complex is thought to proceed to endocytosis via clathrin-coated pits (Law and Loh, 1999; Ferguson, 2001; von Zastrow et al., 2003). The separation of internalization and desensitization has been reported for other G-protein-coupled receptors such as β_2-adrenergic and neurokinin-1 receptors (Pippig et al., 1995; Bennett et al., 2002), but it has also been show that the desensitization of somatostatin and V1b vasopressin receptors requires internalization (Beaumont et al., 1998; Hassan and Mason, 2005). Although this sequence has been established in many heterologous systems, the role of this process in MOR signaling is the subject of some debate. One theory is that the removal of receptors from the plasma membrane by internalization decreases signaling, thus mediating desensitization (Whistler et al., 1999; Finn and Whistler, 2001). Other work suggests that receptor desensitization is augmented when receptors are not removed from the plasma membrane (Koch et al., 2005). Given the differences in results obtained in model systems and the fact that far less work has been done in primary neurons, it is not a surprise that the basic mechanisms underlying desensitization and receptor trafficking in neurons have not been completely characterized (Connor et al., 2004).

The ability to study receptor signaling on single neurons in the absence of internalization was made possible with the use of Derm-A594. The inhibition of G-protein-coupled receptor internalization with concanavalin A is well established (Xiang et al., 2002; Kim et al., 2004). In the present study, experiments using concanavalin A confirmed the absence of internalized Derm-A594. After blockade of internalization, Derm-A594 still caused a hyperpolarization that peaked and declined (desensitized) as in control. Thus, desensitization induced by Derm-A594, a compound that normally is efficient at causing internalization, is completely unaffected after the block of internalization. This experiment also showed that concanavalin A did not interrupt processes such as receptor binding, the coupling to G-proteins, the activation of potassium channels, or the α_2-adrenoreceptor-dependent increase in potassium conductance. This observation confirms work done in AtT20 cells showing that morphine caused desensitization but was poor at inducing internalization (Borgland et al., 2003) and suggests that the desensitization caused by many, if not all, opioid agonists will proceed as normal under conditions where receptor trafficking is disrupted.

Based on experiments done in HEK293 cells expressing epitope-tagged MORs where the recycling of receptors was blocked with monensin, desensitization induced by DAMGO ([D-Ala^2, N-Me-Phe^4, glycinol^5] enkephalin) was increased, whereas that induced by morphine was not affected (Koch et al., 2005). Treatment of brain slices with monensin also increased the degree of desensitization to both ME and an active metabolite of morphine, morphine-6-β-D-glucuronide (Dang and Williams, 2004). It was concluded that internalization plays a role in recovery from desensitization rather than desensitization itself. The present results show that both the onset and recovery from desensitization occurred in preparations where receptor trafficking was blocked with concanavalin A. This observation suggests that the role of receptor endocytosis and recycling is not the only mechanism responsible for either the initial desensitization or recovery. This does not rule out an action on the prolonged recovery from desensitization seen after chronic morphine treatment (Dang and Williams, 2004). It is equally possible that redundant pathways mediate acute desensitization and blocking one mechanism has little effect on the decrease in downstream signaling.

References

Alvarez VA, Arttamangkul S, Dang VC, Salem A, Whistler JL, von Zastrow M, Grandy DK, Williams JT (2002) μ-Opioid receptors: ligand-dependent activation of potassium conductance, desensitization and internalization. J Neurosci 22:5769–5776.

Arttamangkul S, Alvarez-Maubecin V, Thomas G, Williams JT, Grandy DK

(2000) Binding and internalization of fluorescent opioid peptide conjugates in living cells. Mol Pharmacol 58:1570–1580.
Bailey CP, Connor M (2005) Opioids: cellular mechanisms of tolerance and physical dependence. Curr Opin Pharmacol 5:60–68.
Bailey CP, Kelly E, Henderson G (2004) Protein kinase C activation enhances morphine-induced rapid desensitization of mu-opioid receptors in mature rat locus ceruleus neurons. Mol Pharmacol 66:1592–1598.
Beaumont V, Hepworth MB, Luty JS, Kelly E, Henderson G (1998) Somatostatin receptor desensitization in NG108–15 cells. A consequence of receptor sequestration. J Biol Chem 273:33174–33183.
Bennett VJ, Perrine SA, Simmons MA (2002) A novel mechanism of neurokinin-1 receptor resensitization. J Pharmacol Exp Ther 303:1155–1162.
Blanchet C, Luscher C (2002) Desensitization of mu-opioid receptor-evoked potassium currents: initiation at the receptor, expression at the effector. Proc Natl Acad Sci USA 99:4674–4679.
Borgland SL, Connors M, Osborne PB, Furness JB, Christie MJ (2003) Opioid agonists have different efficacy profiles for G protein activation, rapid desensitization, and endocytosis of mu-opioid receptors. J Biol Chem 278:18776–18784.
Celver J, Xu M, Jin W, Lowe J, Chavkin C (2004) Distinct domains of the mu-opioid receptor control uncoupling and internalization. Mol Pharmacol 65:528–537.
Chieng B, Bekkers JM (1999) $GABA_B$, opioid and α_2 receptor inhibition of calcium channels in acutely-dissociated locus coeruleus neurons. Br J Pharmacol 127:1533–1538.
Connor M, Borgland SL, Christie MJ (1999) Continued morphine modulation of calcium channel currents in acutely isolated locus coeruleus neurons from morphine-dependent rats. Br J Pharmacol 128:1561–1569.
Connor M, Osborne PB, Christie MJ (2004) μ-Opioid receptor desensitization: is morphine different? Br J Pharmacol 143:1–12.
Contet C, Kieffer BL, Befort K (2004) Mu opioid receptor: a gateway to drug addiction. Curr Opin Neurobiol 14:370–378.
Dang VC, Williams JT (2004) Chronic morphine treatment reduced recovery from opioid desensitization. J Neurosci 24:7699–7706.
Dang VC, Williams JT (2005) Morphine-induced μ-opioid receptor desensitization. Mol Pharmacol 68:1127–1132.
Ferguson SS (2001) Evolving concepts in G protein-coupled receptor endocytosis: the role in receptor desensitization and signaling. Pharmacol Rev 53:1–24.
Finn AK, Whistler JL (2001) Endocytosis of the mu opioid reduces tolerance and a cellular hallmark of withdrawal. Neuron 32:829–839.
Gainetdinov RR, Premont RT, Bohn LM, Lefkowitz RJ, Caron MG (2004) Desensitization of G protein-coupled receptors and neuronal functions. Annu Rev Neurosci 27:107–144.
Haberstock-Debic H, Kim K, Yu YJ, von Zastrow M (2005) Morphine promotes rapid, arrestin-dependent endocytosis of μ-opioid receptors in striatal neurons. J Neurosci 25:7847–7857.
Hassan A, Mason D (2005) Mechanisms of desensitization of the adrenocorticotropin response to arginine vasopressin in ovine anterior pituitary cells. J Endocrinol 184:29–40.
Ingram S, Wilding TJ, McCleskey EW, Williams JT (1997) Efficiency and kinetics of opioid action on acutely dissociated neurons. Mol Pharmacol 52:136–143.
Johnson MD (1994) Synaptic glutamate release by postnatal rat serotonergic neurons in microculture. Neuron 12:433–442.
Keith DE, Murray SR, Zaki PA, Chu PC, Lissin DV, Kang L, Evans CJ, von Zastrow M (1996) Morphine activates opioid receptors without causing their rapid internalization. J Biol Chem 271:19021–19024.
Kim SJ, Kim MY, Lee EJ, Ahn YS, Baik JH (2004) Distinct regulation of internalization and mitogen-activated protein kinase activation by two isoforms of the dopamine D2 receptor. Mol Endocrinol 18:640–652.
Koch T, Widera A, Bartzsch K, Schulz S, Brandenburg LO, Wundrack N, Beyer A, Grecksch G, Holt V (2005) Receptor endocytosis counteracts the development of opioid tolerance. Mol Pharmacol 67:280–287.
Kovoor A, Celver JP, Wu A, Chavkin C (1998) Agonist induced homologous desensitization of mu-opioid receptors mediated by G protein-coupled receptor kinases is dependent on agonist efficacy. Mol Pharmacol 54:704–711.
Law PY, Loh HH (1999) Regulation of opioid receptor activities. J Pharm Exp Ther 289:607–624.
Lee MC, Cahill CM, Vincent J-P, Beaudet A (2002) Internalization and trafficking of opioid receptor ligands in rat cortical neurons. Synapse 43:102–111.
Masuko S, Nakajima Y, Nakajima S, Yamaguchi K (1986) Noradrenergic neurons from the locus ceruleus in dissociated cell culture: culture methods, morphology and electrophysiology. J Neurosci 6:3229–3241.
Matsushita N, Okada H, Yasoshima Y, Takahashi K, Kiuchi K, Kobayashi K (2002) Dynamics of tyrosine hydroxylase promoter activity during midbrain dopaminergic neuron development. J Neurochem 82:295–304.
Pippig S, Andexinger S, Lohse MJ (1995) Sequestration and recycling of beta 2-adrenergic receptors permit receptor resensitization. Mol Pharmacol 47:666–676.
Pologruto TA, Sabatini BL, Svoboda K (2003) ScanImage: flexible software for operating laser scanning microscopes. Biomed Eng Online 2:13.
Sawamoto K, Nakao N, Kobayashi K, Matsushita N, Takahashi H, Kakishita K, Yamamoto A, Yoshizaki T, Terashima T, Murakami F, Itakura T, Okano H (2001) Visualization, direct isolation and transplantation of midbrain dopaminergic neurons. Proc Natl Acad Sci USA 98:6423–6428.
Sulzer D, Joyce MP, Geldwert D, Haber SN, Hattori T, Rayport S (1998) Dopamine neurons make glutamatergic synapses *in vitro*. J Neurosci 18:4588–4602.
Torrecilla M, Marker CL, Cintora SC, Stoffel M, Williams JT, Wickman K (2002) G-protein-gated potassium channels containing Kir3.2 and Kir3.3 subunits mediate the acute inhibitory effects of opioids on locus ceruleus neurons. J Neurosci 22:4328–4334.
von Zastrow M, Svingos A, Haberstock-Debic H, Evans C (2003) Regulated endocytosis of opioid receptors: cellular mechanisms and proposed roles in physiological adaptation to opiate drugs. Curr Opin Neurobiol 13:348–353.
Whistler JL, Chuang HH, Chu P, Jan LY, von Zastrow M (1999) Functional dissociation of mu opioid receptor signaling and endocytosis: implications for the biology of opiate tolerance and addiction. Neuron 23:737–746.
Williams JT, North RA (1984) Opiate-receptor interactions on single locus coeruleus neurones. Mol Pharmacol 26:489–497.
Williams JT, Christie MJ, North RA (1987) Potentiation of enkephalin action by peptidase inhibitors in rat locus coeruleus in vitro. J Pharmacol Exp Ther 243:397–401.
Williams JT, Christie MJ, Manzoni O (2001) Cellular and synaptic adaptations mediating opioid dependence. Physiol Rev 81:299–343.
Xiang Y, Devic E, Kobilka B (2002) The PDZ binding motif of the beta 1 adrenergic receptor modulates receptor trafficking and signaling in cardiac myocytes. J Biol Chem 277:33783–33790.

LETTERS

Suppression of basal autophagy in neural cells causes neurodegenerative disease in mice

Taichi Hara[1], Kenji Nakamura[2], Makoto Matsui[1,3,4], Akitsugu Yamamoto[5], Yohko Nakahara[2], Rika Suzuki-Migishima[2], Minesuke Yokoyama[6], Kenji Mishima[7], Ichiro Saito[7], Hideyuki Okano[8,9] & Noboru Mizushima[1,10]

Autophagy is an intracellular bulk degradation process through which a portion of the cytoplasm is delivered to lysosomes to be degraded[1–4]. Although the primary role of autophagy in many organisms is in adaptation to starvation, autophagy is also thought to be important for normal turnover of cytoplasmic contents, particularly in quiescent cells such as neurons. Autophagy may have a protective role against the development of a number of neurodegenerative diseases[5–8]. Here we report that loss of autophagy causes neurodegeneration even in the absence of any disease-associated mutant proteins. Mice deficient for *Atg5* (autophagy-related 5) specifically in neural cells develop progressive deficits in motor function that are accompanied by the accumulation of cytoplasmic inclusion bodies in neurons. In $Atg5^{-/-}$ cells, diffuse, abnormal intracellular proteins accumulate, and then form aggregates and inclusions. These results suggest that the continuous clearance of diffuse cytosolic proteins through basal autophagy is important for preventing the accumulation of abnormal proteins, which can disrupt neural function and ultimately lead to neurodegeneration.

Every eukaryotic cell has two main systems for the degradation of intracellular components: the ubiquitin–proteasome system and autophagy. Autophagy is a generic term for the degradation of cellular components in lysosomes[1–4]. Macroautophagy (hereafter referred to as autophagy) is believed to be the main pathway among several subtypes of autophagy. During the process of autophagy, small portions of cytoplasm are sequestered by autophagosomes and then degraded on fusion with lysosomes. In contrast to the ubiquitin–proteasome system, which accounts for most of the selective intracellular protein degradation, autophagy is less selective. Autophagy induced by starvation is a mechanism for producing amino acids within cells. In yeast, autophagy-defective cells are susceptible to starvation. In comparison, mice deficient for Atg5 and Atg7, which are essential for autophagosome formation[9], suffer from severe nutrient- and energy-insufficiency soon after birth[10,11]. Thus, adaptation to starvation is an evolutionarily conserved role of autophagy.

In addition to induced autophagy, a low level of constitutive autophagy is important for intracellular clearance under normal conditions. Mice bearing a liver-specific conditional knockout allele of *Atg7* show hepatic dysfunction and intracellular ubiquitin-positive inclusion bodies[11]. We have also observed the accumulation of ubiquitin-positive inclusion bodies in hepatocytes and a subset of neurons in *Atg5*-knockout ($Atg5^{-/-}$) neonates (Supplementary Fig. S1); however, conventional histological analysis revealed no significant abnormality[10]. These data suggest that intracellular protein quality-control by autophagy is particularly important in neural cells. Indeed, several studies have suggested that impairment of autophagy could worsen the accumulation of abnormal proteins in neurodegenerative disease models *in vitro* and *in vivo*[5–8]. However, direct evidence demonstrating that autophagy contributes to the prevention of neurodegeneration has been lacking, in part because $Atg5^{-/-}$ and $Atg7^{-/-}$ mice die soon after birth[10,11].

To determine the role of autophagy in neural cells, we generated neural-cell-specific $Atg5^{-/-}$ mice (Supplementary Fig. S2). Mice bearing an $Atg5^{flox}$ allele, in which exon 3 of the *Atg5* gene is flanked by two *loxP* sequences, were crossed with a transgenic line expressing Cre recombinase under the control of the nestin promoter (nestin-*Cre*)[12]. In these mice, Cre recombinase is expressed in neural precursor cells after embryonic day (E)10.5, causing deletion of the *loxP*-flanked exon 3 (Supplementary Fig. S3). Recombination was successful in over 90% of all brain cells from $Atg5^{flox/flox}$; nestin-*Cre* mice. The expression of Atg5 (detected as an Atg12–Atg5 conjugate[13]) and the Atg5-dependent conversion of microtubule-associated protein 1 light chain 3 (LC3)-I to LC3-II (LC3–phosphatidylethanolamine (LC3–PE) conjugate)[13,14] were almost completely suppressed in the brains of $Atg5^{flox/flox}$; nestin-*Cre* mice after E15.5 (Fig. 1a and Supplementary Fig. S3). These data suggest that autophagosome formation is impaired in the brains of these mutant mice.

$Atg5^{flox/flox}$; nestin-*Cre* mice were born normally and survived neonatal starvation. They did not show the suckling defects observed in $Atg5^{-/-}$ and $Atg7^{-/-}$ neonates[10,11], suggesting that an undetectable, but sufficient, level of Atg5 remains in the neurons controlling the suckling response at this stage, or that non-neural cells may mediate the suckling deficit in the non-conditional mutants. However, the $Atg5^{flox/flox}$; nestin-*Cre* mice showed growth retardation: their mean body weight was about 1.5-times lower than that of control ($Atg5^{flox/+}$; nestin-*Cre*) mice (Fig. 1b). $Atg5^{flox/flox}$; nestin-*Cre* mice developed progressive motor and behavioural deficits after three weeks of age, and footprint analysis revealed an ataxic walking pattern (Fig. 1c). Mean stride lengths corrected for paw base widths were significantly decreased compared with control ($Atg5^{flox/-}$; nestin-*Cre*) mice. The $Atg5^{flox/flox}$; nestin-*Cre* mice showed limb-clasping reflexes when they were suspended by their tails, whereas control mice extended their limbs (Fig. 1d). This abnormal reflex is often observed in mouse models of neurodegenerative disease[15,16].

[1]Department of Bioregulation and Metabolism, Tokyo Metropolitan Institute of Medical Science, Tokyo 113-8613, Japan. [2]Mouse Genome Technology Laboratory, Mitsubishi Kagaku Institute of Life Sciences, Tokyo 194-8511, Japan. [3]Department of Basic Biology, School of Life Science, the Graduate University for Advanced Studies, Okazaki 444-8585, Japan. [4]Department of Cell Biology, National Institute for Basic Biology, Okazaki 444-8585, Japan. [5]Department of Bio-Science, Nagahama Institute of Bio-Science and Technology, Nagahama 526-0829, Japan. [6]Brain Research Institute, Niigata University, Niigata 951-8510, Japan. [7]Department of Pathology, Tsurumi University School of Dental Medicine, Yokohama 230-8501, Japan. [8]Department of Physiology, Keio University School of Medicine, Tokyo 160-8582, Japan. [9]SORST and [10]PRESTO, Japan Science and Technology Agency, Kawaguchi 332-0012, Japan.

Rotarod (Fig. 1e) and wire-hanging (data not shown) tasks also showed severely impaired motor coordination, balance and grip strength in *Atg5*$^{flox/flox}$; nestin-*Cre* mice. Finally, tremor was apparent in 12-week-old mice. Some of the *Atg5*$^{flox/flox}$; nestin-*Cre* mice died after three weeks of age. Neither *Atg5*$^{flox/flox}$ mice (Cre-negative) nor *Atg5*$^{flox/+}$; nestin-*Cre* mice showed any abnormal phenotype.

The gross anatomy of the brain of the mutant mice was normal. However, histological examination revealed degenerative changes in the neurons of *Atg5*$^{flox/flox}$; nestin-*Cre* mice. These alterations were most prominent in cerebellar Purkinje cells. Haematoxylin and eosin (H&E) staining (arrowheads in Fig. 2a) and immunohistochemical staining with an antibody directed against calbindin (a selective marker for Purkinje cells, left panels in Fig. 2b), demonstrated partial loss of these neurons (Fig. 2c). The remaining Purkinje cells showed eccentrically located nuclei, with infolding of the nuclear membrane. We also found a number of eosinophilic spheroids in H&E-stained sections in the cerebellar nuclei of these mutant mice (arrows in Fig. 2a), which probably correspond to the calbindin-positive spheroids in the same region (Fig. 2b, right panels). These structures suggest massive swelling of Purkinje cell axons that project to the cerebellar nuclei[17,18]. In addition, TUNEL-positive cells were detected in the adjacent granular layer, suggesting apoptosis of granular cells in *Atg5*$^{flox/flox}$; nestin-*Cre* mice (Fig. 2d). Consistent with previous observations, the survival of granular cells largely depends on their synaptic connectivity with Purkinje cells[19]. Axonal swelling was observed in other regions of the *Atg5*$^{flox/flox}$; nestin-*Cre* brain, including the cerebral cortex, the nucleus gracilis (Fig. 2a), the posterior thalamic nucleus, hippocampus, inferior colliculus, trigeminal nucleus, parabranchial nucleus, anterior thalamic nucleus, caudal pons and reticular nucleus (data not shown). Partial loss of pyramidal cells also was observed in the cerebral cortex (data not shown). Together, these data suggest that *Atg5*$^{flox/flox}$; nestin-*Cre* mice suffer from neurodegeneration.

We next examined protein aggregation in the brain using an antibody against ubiquitin, a marker of misfolded proteins. Large, ubiquitin-positive inclusion bodies accumulated in the cytoplasm of large neurons in the thalamus, pons, medulla, dorsal root ganglion (DRG) (Fig. 3a) and midbrain (data not shown) of *Atg5*$^{flox/flox}$; nestin-*Cre* mice. Neurons in the cerebral cortex, hippocampus (especially in the CA3 and CA4 regions) (Fig. 3a), striatum and olfactory bulb (data not shown) were also positive for these inclusion

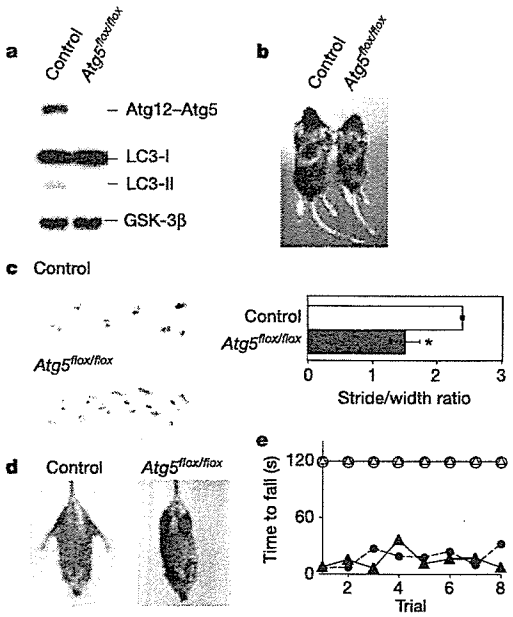

Figure 1 | Behavioural abnormalities in mice lacking *Atg5* in the nervous system. **a**, Immunoblot analysis of Atg5 and LC3. Brain homogenates were prepared from six-week-old control (*Atg5*$^{flox/+}$; nestin-*Cre*) and *Atg5*$^{flox/flox}$; nestin-*Cre* (*Atg5*$^{flox/flox}$) mice. Immunoblot analysis was performed using antibodies against Atg5 and LC3. GSK-3β was used as a loading control. The positions of the Atg12–Atg5 conjugate, LC3-I and LC3-II (LC3–PE conjugate) are indicated. Atg5 monomer was not detected in either lane (data not shown). **b**, A representative male control (*Atg5*$^{flox/+}$; nestin-*Cre*) and an *Atg5*$^{flox/flox}$; nestin-*Cre* (*Atg5*$^{flox/flox}$) littermate at three weeks of age. **c**, Left, paw placement records of eight-week-old mice. Right, stride lengths corrected for paw base widths (stride/width ratio) of *Atg5*$^{flox/flox}$; nestin-*Cre* and control (*Atg5*$^{flox/+}$; nestin-*Cre*) littermate mice. Values represent means ± s.d. of four mice. Asterisk, $P < 0.01$ (Student's *t*-test). **d**, Abnormal limb-clasping of an *Atg5*$^{flox/flox}$; nestin-*Cre* mouse compared with a control mouse (*Atg5*$^{flox/+}$; nestin-*Cre*) when suspended by its tail. **e**, Rotarod testing of *Atg5*$^{flox/+}$; nestin-*Cre* (open symbols) and *Atg5*$^{flox/flox}$; nestin-*Cre* (closed symbols) mice. One male and one female mouse were analysed for each genotype. The time until drop from the rod (rotating at 20 r.p.m.) is shown.

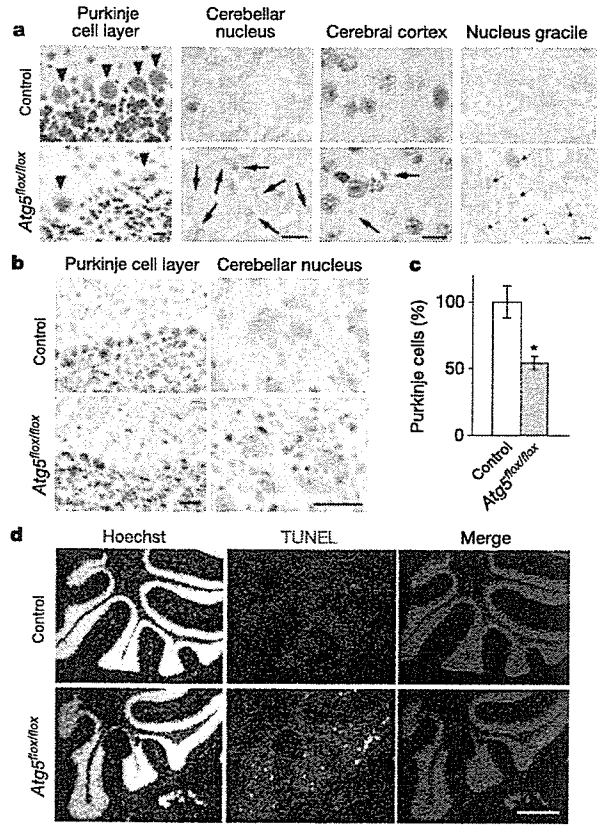

Figure 2 | Neuronal degeneration in *Atg5*$^{flox/flox}$; nestin-*Cre* mice. **a**, H&E-stained sections of the cerebral cortex, the gracile nucleus and cerebellum from control (*Atg5*$^{flox/+}$; nestin-*Cre*) and *Atg5*$^{flox/flox}$; nestin-*Cre* (*Atg5*$^{flox/flox}$) mice at three months of age. Purkinje cells are indicated with arrowheads. Arrows indicate eosinophilic spheroids, which represent axon swelling. Scale bar, 10 μm. **b**, Immunohistochemistry using an anti-calbindin antibody on cerebellum sections from control (*Atg5*$^{flox/+}$; nestin-*Cre*) and *Atg5*$^{flox/flox}$; nestin-*Cre* mice at six weeks of age. Scale bar, 25 μm. **c**, Loss of Purkinje cells in *Atg5*$^{flox/flox}$; nestin-*Cre* mice. Purkinje cells were counted in comparable areas for each mouse, and three fields were counted in each area for each mouse. Data are normalized against values from control mice (*Atg5*$^{flox/+}$; nestin-*Cre*). Values represent mean ± s.d. of three mice. Asterisk, $P < 0.01$ (*t*-test). **d**, Apoptotic death of granular cells. Cerebellum sections from control (*Atg5*$^{flox/+}$; nestin-*Cre*) and *Atg5*$^{flox/flox}$; nestin-*Cre* mice at six weeks of age were subjected to TUNEL staining. Nuclei were stained with Hoechst 33258. Scale bar, 500 μm.

bodies. Such inclusion bodies were not observed in the brains of control (*Atg5*$^{flox/+}$; nestin-*Cre*) mice. We observed ubiquitin-positive inclusion bodies exclusively in cells positive for the neural cell marker NeuN, suggesting that inclusion bodies were generated only in neurons and not in glial cells (Fig. 3b). Notably, although there was extensive loss of Purkinje cells, these neurons had very few inclusion bodies in their cell bodies (Fig. 3a). Numerous ubiquitin-positive dots were observed in the cerebellar nuclei (Fig. 3a), but most of them did not colocalize with the calbindin dots observed in Fig. 2b (data not shown).

The accumulation of inclusion bodies was time-dependent, and the distribution of inclusion-body-positive cells was more limited in *Atg5*$^{-/-}$ and *Atg5*$^{flox/flox}$; nestin-*Cre* newborns compared to adult mice. In *Atg5*$^{-/-}$ neonates, inclusion bodies were observed in the pons, DRG, spinal cord (ventral horn) (Supplementary Fig. S1), hypothalamus, midbrain and trigeminal ganglia (data not shown), but not in the cerebral cortex (Supplementary Fig. S1). A similar pattern was observed in the brain and DRG of *Atg5*$^{flox/flox}$; nestin-*Cre* neonates (Supplementary Fig. S4 and data not shown). Immunoelectron microscopy of DRG neurons isolated from *Atg5*$^{-/-}$ neonates

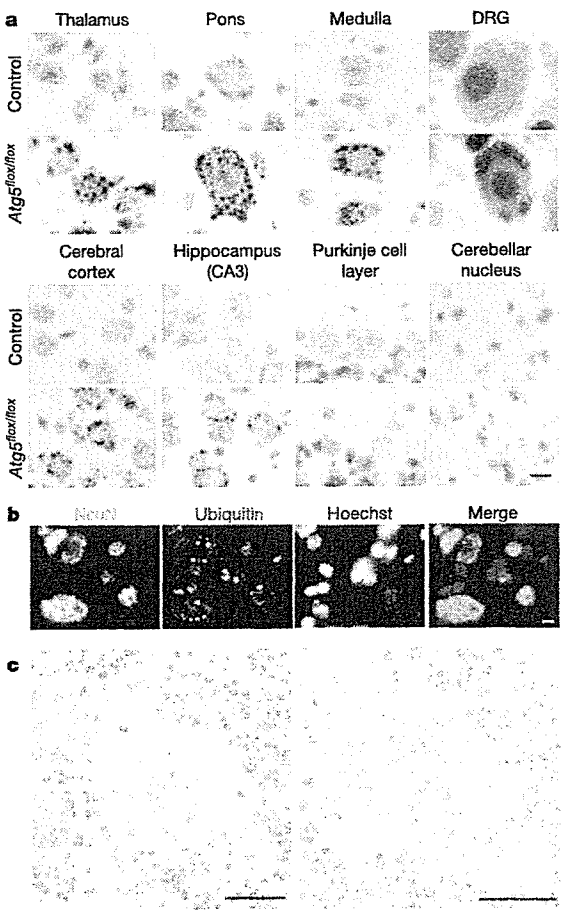

Figure 3 | Ubiquitin-positive inclusions in *Atg5*-deficient neurons. **a**, Immunohistochemistry of brain sections from control (*Atg5*$^{flox/+}$; nestin-*Cre*) and *Atg5*$^{flox/flox}$; nestin-*Cre* (*Atg5*$^{flox/flox}$) mice at six weeks of age, stained with an anti-ubiquitin antibody (1B3). Scale bar, 10 μm. **b**, Ubiquitin-positive inclusions in neurons. Sections of medulla from *Atg5*$^{flox/flox}$; nestin-*Cre* mice at six weeks of age were stained with an antibody against NeuN (a neuron-specific nuclear protein) and ubiquitin. Nuclei were stained with Hoechst 33258. Scale bar, 10 μm. **c**, Immunoelectron microscopy of ubiquitin-positive inclusion bodies. DRG neurons isolated from *Atg5*$^{-/-}$ neonates were analysed by immunoelectron microscopy using an anti-ubiquitin antibody. Scale bars, 500 nm.

demonstrated the specific association of ubiquitin with amorphous, occasionally filamentous, structures (Fig. 3c, left), as well as with more compact structures surrounded by filamentous materials (Fig. 3c, right; see Supplementary Fig. S5 for larger images). Outside the brain, *Atg5*$^{-/-}$ neonates showed inclusion body formation in the liver, the anterior lobe of pituitary gland (Supplementary Fig. S1) and the adrenal gland (data not shown).

Histological examination of *Atg5*$^{-/-}$ and *Atg5*$^{flox/flox}$; nestin-*Cre* mice suggested that, in addition to the presence of inclusion bodies, the intensity of diffuse cytoplasmic ubiquitin staining was higher compared with wild-type mice. We thus analysed the time course of accumulation of diffuse ubiquitinated proteins and inclusions in DRG neurons (the neonatal tissue in which inclusion body formation was most striking). DRG neurons from *Atg5*$^{-/-}$ embryos at E13.5 had no apparent abnormality. However, at E15.5, some neurons had accumulated diffuse, cytosolic ubiquitinated proteins with infrequent inclusions (Fig. 4a). Later, in newborn (postnatal day (P)0) *Atg5*$^{-/-}$ mice, multiple ubiquitin-positive inclusion bodies were present in DRG neurons. Thus, the accumulation of diffuse abnormal proteins seems to be the primary cellular phenotype of *Atg5*$^{flox/flox}$; nestin-*Cre* neurons. We obtained similar results using a biochemical method with whole brains. Polyubiquitinated proteins that accumulated in *Atg5*$^{flox/flox}$; nestin-*Cre* brains were primarily Triton-soluble in six-week-old mice (Fig. 4b). In contrast, in 14-week-old mice, Triton-insoluble polyubiquitinated proteins were also abundant, suggesting that inclusion body formation is a later event.

We confirmed these observations using hepatocytes, another cell type that showed extensive inclusion body accumulation under autophagy-defective conditions[11] (Supplementary Fig. S1). We crossed *Atg5*$^{flox/flox}$ mice with CAG-*Cre* mice that express Cre recombinase ubiquitously (see Methods)[20]. As recombination efficiency was not high when crossed with our *Atg5*$^{flox/flox}$ mice, the resulting mice (*Atg5*$^{flox/flox}$; CAG-*Cre*) were mosaic for the mutant allele and viable. In the livers of these mice, the *Atg5* gene was deleted in only about 30% of hepatocytes (Supplementary Fig. S6), which allowed us to compare directly the immunoreactivity of knockout cells with that of wild-type cells in the same specimen. Anti-ubiquitin staining of the liver in four-month-old *Atg5*$^{flox/flox}$; CAG-*Cre* mice showed that about 30% of cells had very high levels of diffuse cytoplasmic signals (in addition to inclusion bodies), compared with surrounding cells that were probably wild type (Fig. 4c). The results clearly demonstrate that cytosolic ubiquitinated proteins also accumulate in *Atg5*$^{-/-}$ hepatocytes.

We then determined the time course of accumulation of ubiquitinated proteins using Mx1-*Cre* transgenic mice[21]. In this system, Cre recombinase is expressed under the control of an interferon-responsive promoter that can be activated by application of polyinosinic acid-polycytidylic acid (pIpC), an interferon-inducible, synthetic double-stranded RNA. The *Atg5* gene in *Atg5*$^{flox/flox}$; Mx1-*Cre* liver was deleted by intraperitoneal injection of pIpC. Soon after injection, most targeted cells showed only diffuse ubiquitin staining, with no inclusion bodies (Fig. 4d, e). In contrast, large, ubiquitin-positive inclusion bodies were present in almost all targeted hepatocytes 16 days after pIpC injection (arrowheads in Fig. 4d). Cells with only inclusion bodies but not diffuse cytoplasmic staining were observed very rarely. Taken together, our data demonstrate that loss of autophagy first leads to accumulation of diffuse abnormal proteins, followed by generation of inclusion bodies.

We have shown that the inhibition of autophagy in neural cells causes neurodegeneration and symptoms of neurological pathology. As the mouse model we used does not express any disease-associated mutant proteins, the phenotype of these mutant mice indicates that autophagy mediates essential and continuous turnover of intracellular proteins. This system is particularly important for neurons, in which deregulation of this degradation process can induce cell dysfunction. The role of autophagy could be even more critical if

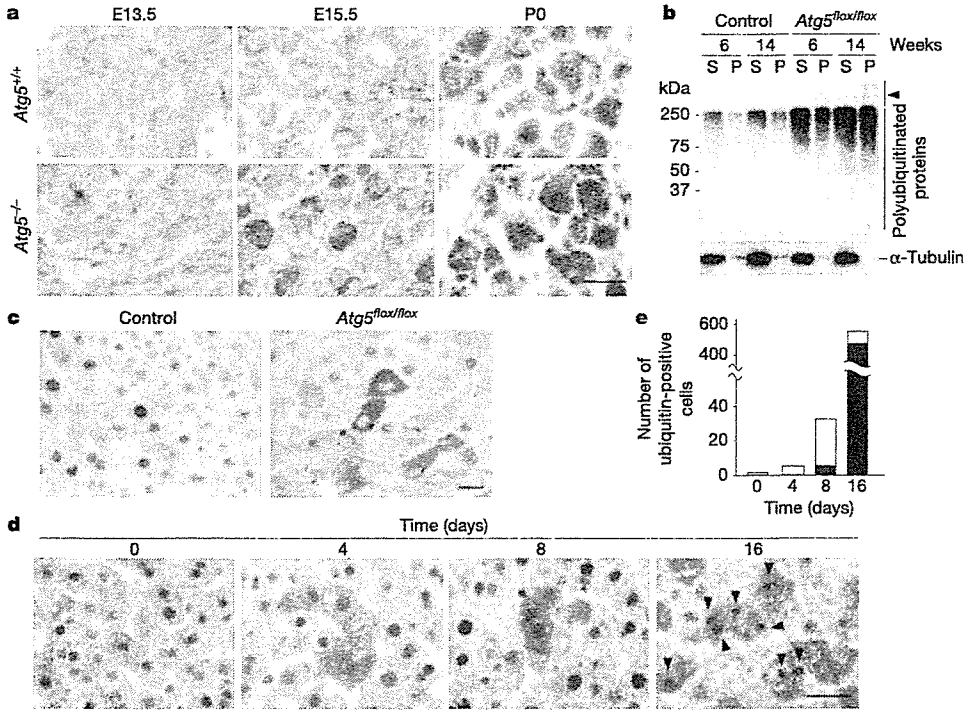

Figure 4 | Accumulation of diffuse ubiquitinated proteins in autophagy-defective cells. **a**, Immunohistochemistry of DRG neurons from $Atg5^{+/+}$ and $Atg5^{-/-}$ mice at different developmental stages (embryonic day (E)13.5, E15.5 or postnatal day (P)0), stained with an antibody directed against ubiquitin. Scale bar, 25 μm. **b**, Accumulation of Triton-X-100-soluble polyubiquitinated proteins in the brains of $Atg5^{flox/flox}$; nestin-*Cre* mice. Brain homogenate prepared at the indicated times from control ($Atg5^{flox/+}$; nestin-*Cre*) and $Atg5^{flox/flox}$; nestin-*Cre* ($Atg5^{flox/flox}$) mice were separated into Triton-X-100-soluble (S) and -insoluble (P) fractions and analysed by immunoblotting using anti-ubiquitin antibodies. Arrowhead indicates the stacking gel. **c**, Immunohistochemistry of liver sections from control ($Atg5^{flox/+}$; CAG-*Cre*) and $Atg5^{flox/flox}$; CAG-*Cre* ($Atg5^{flox/flox}$) mice at four months of age, using an anti-ubiquitin antibody. Scale bar, 25 μm. **d**, Immunohistochemistry of liver sections from six-week-old $Atg5^{flox/flox}$; Mx1-*Cre* mice at the indicated time points after pIpC injection, using anti-ubiquitin antibodies. Arrowheads indicate ubiquitin-positive inclusion bodies. Scale bar, 25 μm. **e**, Five thousand hepatocytes were randomly selected, and the number of cells with diffuse cytosolic ubiquitin signals, with (black) or without (white) inclusion bodies, were counted.

any aggregation-prone mutant proteins were expressed. Although autophagy is generally thought to be a non-selective process, several studies have suggested that autophagosomes can specifically engulf inclusion bodies[8,22]. In our system, however, inclusion bodies appeared in later phases of autophagy deficiency, suggesting that the primary role of autophagy under normal conditions is the turnover of diffuse cytosolic proteins, not direct elimination of inclusion bodies. As the population of ubiquitinated proteins in $Atg5^{flox/flox}$; nestin-*Cre* brains was similar to that in wild-type mouse brains, we suggest that cytoplasmic proteins that are usually ubiquitinated, rather than specific proteins, accumulate in larger amounts in the absence of autophagy (Supplementary Fig. S7). Downregulation of protein turnover could cause the accumulation of abnormal proteins, which then could promote aggregate formation (Supplementary Fig. S8).

The critical role of autophagy in the basal turnover of diffuse cytosolic proteins in neural cells should be emphasized, because it has been suggested that large inclusion bodies themselves might not be pathogenic, but that mutant proteins present diffusely in the cytosol could be the primary source of toxicity[23–27]. However, we do not rule out the possibility that autophagosomes can selectively recognize abnormal soluble proteins or microaggregates on the membrane surface. It was recently reported that the polyubiquitin-binding protein p62/SQSTM1 might mediate the specific recognition of protein aggregates by autophagosomes[28]. This pathway might also be involved in the degradation of diffuse ubiquitinated proteins by autophagy.

METHODS

Generation of tissue-specific *Atg5*-deficient mice. An approximately 1-kb *Xba*I–*Spe*I mouse genomic fragment containing putative exon 3 of the *Atg5* gene was flanked by two *loxP* sites containing the neomycin-resistant (*neo*^{r}) cassette from pMC1-Neo (Stratagene). The diphtheria toxin A (*DT-A*) gene was inserted downstream of the short arm, for negative selection against random integration of the vector (Supplementary Fig. S2). Targeted CCE embryonic stem cells of 129/SvEv mouse origin were injected into C57BL/6 blastocysts, and chimaeric mice were crossed with C57BL/6 mice to obtain $Atg5^{flox/+}$ mice. We used the following primers to detect wild-type *Atg5* and $Atg5^{flox}$ alleles: A (exon3-1), 5′-GAATATGAAGGCACACCCCTGAAATG-3′; B (short2), 5′-GTACTGCATAATGGTTTAACTCTTGC-3′; C (check2), 5′-ACAACGTCGAG CACAGCTGCGCAAGG-3′; D (5L2), 5′-CAGGGAATGGTGTCTCCCAC-3′; E (cre1), 5′-AGGTTCGTTCACTCATGGA-3′; F (cre2), 5′-TCGACCAGTTT AGTTACCC-3′.

Southern blot analysis was performed using the probe shown in Supplementary Fig. S2 after digestion of genomic DNA with *Eco*RV and *Kpn*I, as described previously[15]. Nestin-*Cre* transgenic mice expressing Cre recombinase under the control of the mouse nestin gene promoter and second intronic neural enhancer (a gift from S. Noguchi) have been described previously[29]. CAG-*Cre* transgenic mice expressing Cre recombinase under the control of the CAG (CMV enhancer and chicken β-actin) promoter have been described previously[20]. Mx1-*Cre* transgenic mice were obtained from the Jackson Laboratory[21]. Progeny containing the $Atg5^{flox}$ allele were bred with these *Cre* transgenic mice to generate $Atg5^{flox/flox}$; nestin-*Cre*, $Atg5^{flox/flox}$; CAG-*Cre* and $Atg5^{flox/flox}$; Mx1-*Cre* mice. $Atg5^{-/-}$ mice have been described previously[10]. All animal experiments were approved by the institutional committee of the Tokyo Metropolitan Institute of Medical Science.

Antibodies. A monoclonal antibody against ubiquitin (1B3) was purchased from

MBL and used for immunohistochemistry. Rabbit anti-ubiquitin polyclonal antibody (DakoCytomation) was used for immunoelectron microscopy. Anti-polyubiquitin monoclonal antibody (FK2, Nippon Bio-Test Laboratories) was used in immunoblot analyses. The following antibodies were also used: anti-NeuN monoclonal antibody (Chemicon), rabbit anti-calbindin polyclonal antibody (Chemicon), Alexa Fluor 488- and 660-conjugated goat anti-rabbit IgG (H + L) antibodies (Molecular Probes), monoclonal anti-glycogen synthase kinase-3β antibody (BD Biosciences), monoclonal anti-α-tubulin antibody (DM1A, Sigma-Aldrich), and antibodies against Atg5 (SO4)[13] and LC3[14].

Behavioural analysis. Mice were placed on a rod rotating at 20 r.p.m., and the time taken for them to fall from the rod was measured. If a mouse stayed on the rod until the end of the 2-min trial, a time of 120 s was recorded.

Immunohistochemical analysis. Mice were transcardially perfused with 4% paraformaldehyde in phosphate buffer (pH 7.4). Tissues were post-fixed in the same fixative overnight and embedded in paraffin. Sections were stained using Meyer's H&E. For immunohistochemical analysis, all tissue sections were subjected to antigen retrieval using the microwave method (in 0.01 M citrate buffer for 10 min). After blocking, sections were incubated with primary antibodies for 1 h, followed by 30 min incubation with fluorescently labelled or biotinylated secondary antibodies that were detected using Histomouse-plus kits (Zymed Laboratories) and the Liquid DAB substrate chromogen system (DakoCytomation). Apoptotic cells were detected by TUNEL assay using an *in situ* cell death detection kit (Roche Diagnostic).

Immunoelectron microscopy. For immunoelectron microscopy, the post-embedding immuno-gold method was used to label tissue sections embedded with LR white resin (London Resin Co.) as previously described[30].

Preparation of detergent-soluble and -insoluble fractions. Mouse brains were homogenized in five volumes of ice-cold 0.25 M sucrose buffer (50 mM Tris-HCl pH 7.4, 1 mM EDTA) with protease inhibitors. Homogenates were centrifuged at 500*g* for 10 min at 4 °C, and the resulting supernatants were lysed with an equal volume of cold sucrose buffer containing 1% Triton X-100. Lysates were subjected to centrifugation at 13,000*g* for 15 min at 4 °C to separate supernatants (fractions soluble in 0.5% Triton-X-100) and pellets. Pellets were resuspended in 1% SDS in PBS (Triton-X-100-insoluble fractions).

Received 6 February; accepted 20 March 2006.
Published online 19 April 2006.

1. Cuervo, A. M. Autophagy: in sickness and in health. *Trends Cell Biol.* 14, 70–77 (2004).
2. Levine, B. & Klionsky, D. J. Development by self-digestion: molecular mechanisms and biological functions of autophagy. *Dev. Cell* 6, 463–477 (2004).
3. Klionsky, D. J. The molecular machinery of autophagy: unanswered questions. *J. Cell Sci.* 118, 7–18 (2005).
4. Mizushima, N. The pleiotropic role of autophagy: from protein metabolism to bactericide. *Cell Death Differ.* 12, 1535–1541 (2005).
5. Ravikumar, B., Duden, R. & Rubinsztein, D. C. Aggregate-prone proteins with polyglutamine and polyalanine expansions are degraded by autophagy. *Hum. Mol. Genet.* 11, 1107–1117 (2002).
6. Fortun, J., Dunn, W. A. Jr, Joy, S., Li, J. & Notterpek, L. Emerging role for autophagy in the removal of aggresomes in Schwann cells. *J. Neurosci.* 23, 10672–10680 (2003).
7. Ravikumar, B. *et al.* Inhibition of mTOR induces autophagy and reduces toxicity of polyglutamine expansions in fly and mouse models of Huntington disease. *Nature Genet.* 36, 585–595 (2004).
8. Iwata, A. *et al.* Increased susceptibility of cytoplasmic over nuclear polyglutamine aggregates to autophagic degradation. *Proc. Natl Acad. Sci. USA* 102, 13135–13140 (2005).
9. Mizushima, N., Ohsumi, Y. & Yoshimori, T. Autophagosome formation in mammalian cells. *Cell Struct. Funct.* 27, 421–429 (2002).
10. Kuma, A. *et al.* The role of autophagy during the early neonatal starvation period. *Nature* 432, 1032–1036 (2004).
11. Komatsu, M. *et al.* Impairment of starvation-induced and constitutive autophagy in *Atg7*-deficient mice. *J. Cell Biol.* 169, 425–434 (2005).
12. Betz, U. A., Vosshenrich, C. A., Rajewsky, K. & Muller, W. Bypass of lethality with mosaic mice generated by Cre–*loxP*-mediated recombination. *Curr. Biol.* 6, 1307–1316 (1996).
13. Mizushima, N. *et al.* Dissection of autophagosome formation using Apg5-deficient mouse embryonic stem cells. *J. Cell Biol.* 152, 657–667 (2001).
14. Kabeya, Y. *et al.* LC3, a mammalian homologue of yeast Apg8p, is localized in autophagosome membranes after processing. *EMBO J.* 19, 5720–5728 (2000).
15. Cote, F., Collard, J. F. & Julien, J. P. Progressive neuronopathy in transgenic mice expressing the human neurofilament heavy gene: a mouse model of amyotrophic lateral sclerosis. *Cell* 73, 35–46 (1993).
16. Mangiarini, L. *et al.* Exon 1 of the *HD* gene with an expanded CAG repeat is sufficient to cause a progressive neurological phenotype in transgenic mice. *Cell* 87, 493–506 (1996).
17. Kikuchi, T., Mukoyama, M., Yamazaki, K. & Moriya, H. Axonal degeneration of ascending sensory neurons in gracile axonal dystrophy mutant mouse. *Acta Neuropathol. (Berl.)* 80, 145–151 (1990).
18. Sotelo, C. Axonal abnormalities in cerebellar Purkinje cells of the 'hyperspiny Purkinje cell' mutant mouse. *J. Neurocytol.* 19, 737–755 (1990).
19. Lossi, L., Mioletti, S. & Merighi, A. Synapse-independent and synapse-dependent apoptosis of cerebellar granule cells in postnatal rabbits occur at two subsequent but partly overlapping developmental stages. *Neuroscience* 112, 509–523 (2002).
20. Sakai, K. & Miyazaki, J. A transgenic mouse line that retains Cre recombinase activity in mature oocytes irrespective of the *cre* transgene transmission. *Biochem. Biophys. Res. Commun.* 237, 318–324 (1997).
21. Kuhn, R., Schwenk, F., Aguet, M. & Rajewsky, K. Inducible gene targeting in mice. *Science* 269, 1427–1429 (1995).
22. Kopito, R. R. Aggresomes, inclusion bodies and protein aggregation. *Trends Cell Biol.* 10, 524–530 (2000).
23. Saudou, F., Finkbeiner, S., Devys, D. & Greenberg, M. E. Huntingtin acts in the nucleus to induce apoptosis but death does not correlate with the formation of intranuclear inclusions. *Cell* 95, 55–66 (1998).
24. Kuemmerle, S. *et al.* Huntington aggregates may not predict neuronal death in Huntington's disease. *Ann. Neurol.* 46, 842–849 (1999).
25. Taylor, J. P. *et al.* Aggresomes protect cells by enhancing the degradation of toxic polyglutamine-containing protein. *Hum. Mol. Genet.* 12, 749–757 (2003).
26. Arrasate, M., Mitra, S., Schweitzer, E. S., Segal, M. R. & Finkbeiner, S. Inclusion body formation reduces levels of mutant huntingtin and the risk of neuronal death. *Nature* 431, 805–810 (2004).
27. Tanaka, M. *et al.* Aggresomes formed by α-synuclein and synphilin-1 are cytoprotective. *J. Biol. Chem.* 279, 4625–4631 (2004).
28. Bjorkoy, G. *et al.* p62/SQSTM1 forms protein aggregates degraded by autophagy and has a protective effect on huntingtin-induced cell death. *J. Cell Biol.* 171, 603–614 (2005).
29. Mori, H. *et al.* Socs3 deficiency in the brain elevates leptin sensitivity and confers resistance to diet-induced obesity. *Nature Med.* 10, 739–743 (2004).
30. Yamamoto, A. *et al.* Stacks of flattened smooth endoplasmic reticulum highly enriched in inositol 1,4,5-trisphosphate ($InsP_3$) receptor in mouse cerebellar Purkinje cells. *Cell Struct. Funct.* 16, 419–432 (1991).

Supplementary Information is linked to the online version of the paper at www.nature.com/nature. A summary figure is also included.

Acknowledgements We thank H. Neko, M. Miwa and Y. Kabeya for technical assistance. We also thank J. Miyazaki for the donation of CAG-*Cre* transgenic mice, T. Yoshimori for the anti-LC3 antibody, E. Yamada for histological examination, M. Yuzaki for the rotarod analysis, and A. Kuma for discussion. We thank Z. Yue for critical reading of the manuscript. This work was supported in part by Grants-in-Aid for Scientific Research from the Ministry of Education, Culture, Sports, Science and Technology of Japan. The authors thank the Yamada Science Foundation and the Cell Science Research Foundation for their financial support.

Author Contributions T.H. performed most of the experiments to characterize the neuron-specific knockout mice. M.M. analysed *Atg5* $^{-/-}$ mice. K.N., Y.N., R.S.-M. and M.Y. generated $Atg5^{flox}$ chimaeric mice. A.Y. performed electron microscopy. K.M. and I.S. performed histological analysis. H.O. provided nestin-*Cre* mice and participated in manuscript preparation. N.M. conceived the experiments and generated the targeting vector. T.H. and N.M. wrote the paper.

Author Information Reprints and permissions information is available at npg.nature.com/reprintsandpermissions. The authors declare no competing financial interests. Correspondence and requests for materials should be addressed to to N.M. (nmizu@rinshoken.or.jp).

PNAS
Proceedings of the National Academy of Sciences of the United States of America www.pnas.org

A carbohydrate-binding protein, Galectin-1, promotes proliferation of adult neural stem cells

Masanori Sakaguchi, Tetsuro Shingo, Takuya Shimazaki, Hirotaka James Okano, Mieko Shiwa, Satoru Ishibashi, Hideyuki Oguro, Mikiko Ninomiya, Toshihiko Kadoya, Hidenori Horie, Akira Shibuya, Hidehiro Mizusawa, Françoise Poirier, Hiromitsu Nakauchi, Kazunobu Sawamoto, and Hideyuki Okano

PNAS 2006;103;7112-7117; originally published online Apr 24, 2006;
doi:10.1073/pnas.0508793103

A carbohydrate-binding protein, Galectin-1, promotes proliferation of adult neural stem cells

Masanori Sakaguchi[a,b], Tetsuro Shingo[c], Takuya Shimazaki[a], Hirotaka James Okano[a], Mieko Shiwa[d], Satoru Ishibashi[e], Hideyuki Oguro[f], Mikiko Ninomiya[a,g,h], Toshihiko Kadoya[i], Hidenori Horie[j], Akira Shibuya[b], Hidehiro Mizusawa[e], Françoise Poirier[k], Hiromitsu Nakauchi[f], Kazunobu Sawamoto[a,h], and Hideyuki Okano[a,l]

[a]Department of Physiology and [h]Bridgestone Laboratory of Developmental and Regenerative Neurobiology, Keio University School of Medicine, Tokyo 160-8582, Japan; [b]Institute of Basic Medical Sciences, University of Tsukuba, Ibaraki 305-8575, Japan; [c]Department of Neurological Surgery, Okayama University Graduate School of Medicine and Dentistry, Okayama 700-8558, Japan; [d]Yokohama Laboratory, Ciphergen Biosystems KK, Kanagawa 204-0005, Japan; [e]Department of Neurology and Neurological Science, Graduate School of Medicine, Tokyo Medical and Dental University, Tokyo 113-8596, Japan; [f]Laboratory of Stem Cell Therapy, Center for Experimental Medicine, Institute of Medical Sciences, University of Tokyo, Tokyo 108-8639, Japan; [g]Department of Neurology, Saitama Medical School, Saitama 350-0495, Japan; [i]CMC R&D Laboratories, Pharmaceutical Division, Kirin Brewery, Gunma 370-0013, Japan; [j]Advanced Research Center for Biological Science, Waseda University, Tokyo 202-0021, Japan; and [k]Institut Jacques Monod, Unité Mixte de Recherche Centre National de la Recherche Scientifique 7592, Universities Paris 6 and Paris 7, Cedex 05 Paris, France

Edited by Fred H. Gage, The Salk Institute for Biological Studies, San Diego, CA and approved March 15, 2006 (received for review October 8, 2005)

In the subventricular zone of the adult mammalian forebrain, neural stem cells (NSCs) reside and proliferate to generate young neurons. We screened factors that promoted the proliferation of NSCs *in vitro* by a recently developed proteomics technique, the ProteinChip system. In this screen, we identified a soluble carbohydrate-binding protein, Galectin-1, as a candidate. We show herein that Galectin-1 is expressed in a subset of slowly dividing subventricular zone astrocytes, which includes the NSCs. Based on results from intraventricular infusion experiments and phenotypic analyses of knockout mice, we demonstrate that Galectin-1 is an endogenous factor that promotes the proliferation of NSCs in the adult brain.

lectin | mobilization | stem cell niche

Recently, neural stem cells (NSCs) residing in the adult CNS have been studied to elucidate the mechanisms of ongoing tissue maintenance (1) and to develop strategies for regenerating the damaged CNS (2, 3).

Two neurogenic regions have been identified in the forebrain (FB): the subventricular zone (SVZ) of the lateral ventricle (LV) (4–6) and the subgranular layer of the hippocampal dentate gyrus (7–9). NSCs in these regions can generate functional neurons in the adult brain (10–12). Clinically, soluble factors that regulate these progenitor cells may be useful for regenerating the damaged CNS (13). The identification of additional factors that promote the proliferation of stem cells will contribute to NSC biology and to the development of innovative strategies for brain repair.

The proliferation and differentiation of various adult stem cells are regulated by common soluble factors (14). OP9 is a cell line that has been used to screen for factors that support hematopoietic stem cells (HSCs) (15, 16). In the present study, we found that OP9 conditioned medium (CM) promoted neurosphere formation, by which the proliferation of NSCs can be monitored *in vitro* (17). Using the ProteinChip system (18), we identified Galectin-1 as one of the molecules responsible for this activity.

Galectin-1 is a soluble carbohydrate-binding protein (19, 20) that has been implicated in a variety of biological events (21, 22). Carbohydrates on the cell surface may be involved in the intercellular interactions of various stem cells, including NSCs (23–25) and HSCs (26). A recent report suggested that Galectin-1 promotes the proliferation of HSCs *in vitro* (27). However, its functions in NSCs remain unknown. Here, we report on the expression and function of Galectin-1 in the adult mammalian brain.

Results and Discussion

Galectin-1 Was Found in OP9CM. To examine how OP9 cells affect the proliferation of NSCs, we cultured neurosphere cells (17) with or without OP9CM. At a density of one cell per well, no neurospheres formed in cultures grown without OP9CM (Fig. 1*A*, Ctrl; $n = 800$ cells) (28). In contrast, at the same culture density, of the total cells grown with OP9CM ($n = 400$), 49 ($12.4 \pm 0.54\%$) initiated neurosphere formation (Fig. 1*A*, OP9). Interestingly, the CM from OP9 cells that were passaged repeatedly over 6 months (inactivated OP9, IA-OP9) did not support neurosphere formation (Fig. 1*A*, IA-OP9; $n > 800$).

To identify the OP9-derived molecules that enhanced neurosphere formation, we used an expression screen based on mass spectrometry (18) to detect molecules that were more abundant in OP9CM than in IA-OP9CM. A signal at ≈14.6 kDa showed a reproducible difference in peak height between the two CMs (Fig. 5, which is published as supporting information on the PNAS web site). This fraction was purified, concentrated, and separated by SDS/PAGE, and the band was cut from the gel and analyzed by tandem mass spectrometry (see *Materials and Methods*). We obtained two amino acid sequences (VRGEVASDAK and EDGTWGTEHR) that were identical to portions of the Galectin-1 protein ($n = 3$), suggesting that the 14.6-kDa peak was Galectin-1. Western blotting with a specific Ab showed that the OP9CM contained more Galectin-1 than did the IA-OP9CM ($n = 3$; $P < 0.01$).

Adding recombinant Galectin-1 protein (10 and 100 ng/ml) to the culture medium enhanced the formation of neurospheres cultured at 100 cells per well (Fig. 1*B*; $P < 0.01$, ANOVA). Galectin-1 did not mimic the full activity of the OP9CM, suggesting that there are other factors that enhance neurosphere formation in the OP9CM. The neurospheres grown with Galectin-1 (100 ng/ml) were larger (Fig. 6*A*, which is published as supporting information on the PNAS web site; $P < 0.05$), formed more secondary neurospheres (Fig. 6*B*; $P < 0.05$), and differentiated into neurons, astrocytes, and oligodendrocytes (Fig. 1*C*). Together, these results suggest that Galectin-1 is one of the factors in OP9CM that enhances neurosphere formation.

Expression of Galectin-1 in the Adult Mouse FB. To investigate the *in vivo* function of Galectin-1, we examined its expression in the

---

Conflict of interest statement: No conflicts declared.

This paper was submitted directly (Track II) to the PNAS office.

Freely available online through the PNAS open access option.

Abbreviations: SVZ, subventricular zone; LV, lateral ventricle; FB, forebrain; GFAP, glial fibrillary acidic protein; PCNA, proliferating cell nuclear antigen; NSC, neural stem cell; CM, conditioned medium; IA-OP9, inactivated OP9.

[l]To whom correspondence should be addressed at: Department of Physiology, Keio University School of Medicine, 35 Shinano-machi, Shinjuku-ku, Tokyo 160-8582, Japan. E-mail: hidokano@sc.itc.keio.ac.jp.

www.pnas.org/cgi/doi/10.1073/pnas.0508793103

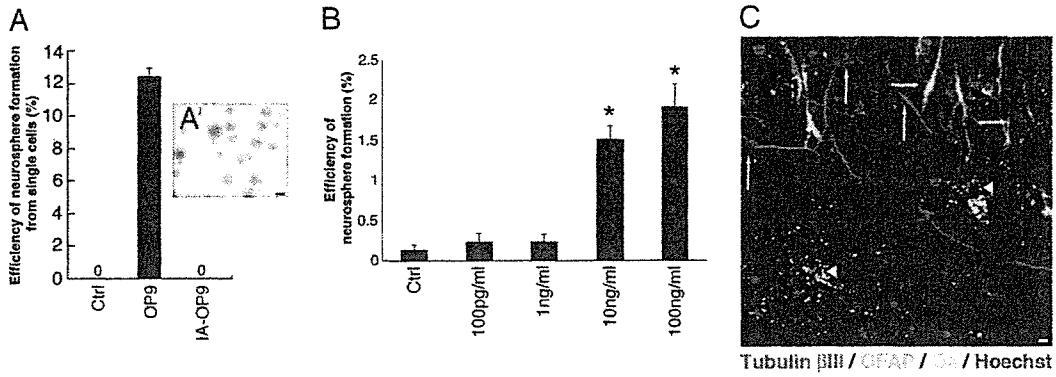

Fig. 1. Galectin-1 enhances neurosphere formation. (*A*) Effects of CM on neurosphere formation. Ctrl, control. (*A'*) The neurospheres initiated by OP9CM could be passaged more than five times. (*B*) Galectin-1 enhances neurosphere formation. Note that some neurospheres formed in the control cultures under this condition (culture density of 100 cells per well). *, $P < 0.01$. (*C*) The neurospheres initiated by Galectin-1 differentiated into neurons and glial cells. Representative images of differentiated cells from a neurosphere generated with recombinant Galectin-1 and immunostained with each neural lineage marker are shown. Tubulin βIII (neurons, red, white arrows), GFAP (astrocytes, green, green arrows), O4 (oligodendrocytes, light blue, arrowheads), and Hoechst (nucleus, dark blue) images were obtained by confocal laser microscopy. (Scale bars: *A*, 100 μm; *C*, 10 μm.)

mouse brain by using a Galectin-1-specific Ab (29). To confirm the specificity and sensitivity of the staining procedures, brain sections from a *galectin-1*-null mutant mouse (30) were simultaneously incubated with the same anti-Galectin-1 Ab, and we observed no staining (Fig. 7, which is published as supporting information on the PNAS web site).

In the adult mouse FB, as reported previously (31), subsets of neurons in the cortex were Galectin-1$^+$ (Fig. 7*A'*). In addition, we found Galectin-1 staining signals in the SVZ (Fig. 7*A''*) and dentate gyrus (Fig. 8*A*, which is published as supporting information on the PNAS web site), the two major adult neurogenic regions. RT-PCR analysis also showed that Galectin-1 is expressed in the SVZ (Fig. 8*B*). Almost all of the Galectin-1$^+$ cells in the adult SVZ expressed glial fibrillary acidic protein (GFAP) (Fig. 2*A*; see Fig. 8*C* for the confocal image), Nestin (Fig. 8*D*), and S100β (Fig. 8*E*). Some of these Galectin-1$^+$ cells were positive for Ki67 (Fig. 8*F*) (32), a nuclear marker of cellular replication. With regard to Galectin-1 expression in GFAP$^+$ cells outside the SVZ, we found that subsets of GFAP$^+$ cells in the subgranular layer and hilus were Galectin-1$^+$ (Fig. 8*A*), whereas most of the GFAP$^+$ cells in the cortex and striatum were Galectin-1$^-$ (Fig. 8 *G* and *H*). In the SVZ, the GFAP$^+$ astrocytes (type B cells) have been shown to act as NSCs (33, 34), which generate Dlx$^+$/Mash1$^+$ type C cells (35, 36) (Toida Kazunori, personal communication) and subsequently differentiate into PSA-NCAM$^+$/Dlx$^+$/Mash1$^-$ type A cells (in which PSA-NCAM is the polysialylated neural cell adhesion molecule) (35, 36). Among striatal neurons (Fig. 8*I*), Mash1$^+$ type C cells, and PSA-NCAM$^+$ type A cells (Fig. 8*J*), none showed Galectin-1 immunoreactivity. Dissociated SVZ cells were stained with

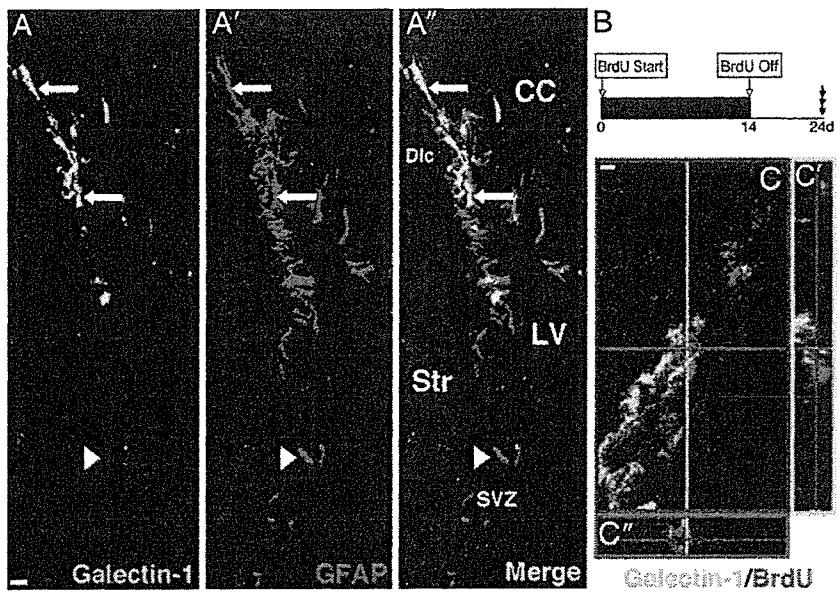

Fig. 2. Galectin-1 is detected in SVZ astrocytes. (*A*) Low-magnification images of Galectin-1 (*A*) and GFAP (*A'*) double immunostaining in the coronal section through the LV. Galectin-1 and GFAP double-positive cells are seen in the SVZ (arrows). Note there are some Galectin-1-negative cells among the GFAP$^+$ cells (e.g., arrowhead). (*A''*) Merged image. CC, corpus callosum; Str, striatum; Dlc, dorsolateral corner. (*B*) Experimental schema for marking slowly dividing cells. (*C*) Slowly dividing Galectin-1$^+$ cell. High-magnification confocal image of a Galectin-1 (green in cell soma) and BrdU (red in nucleus) double-positive cell in the SVZ. Sections were made after 2 weeks of oral BrdU administration followed by 10 days of wash-out. (*C'* and *C''*) 3D reconstruction images. (Scale bars: 5 μm.)

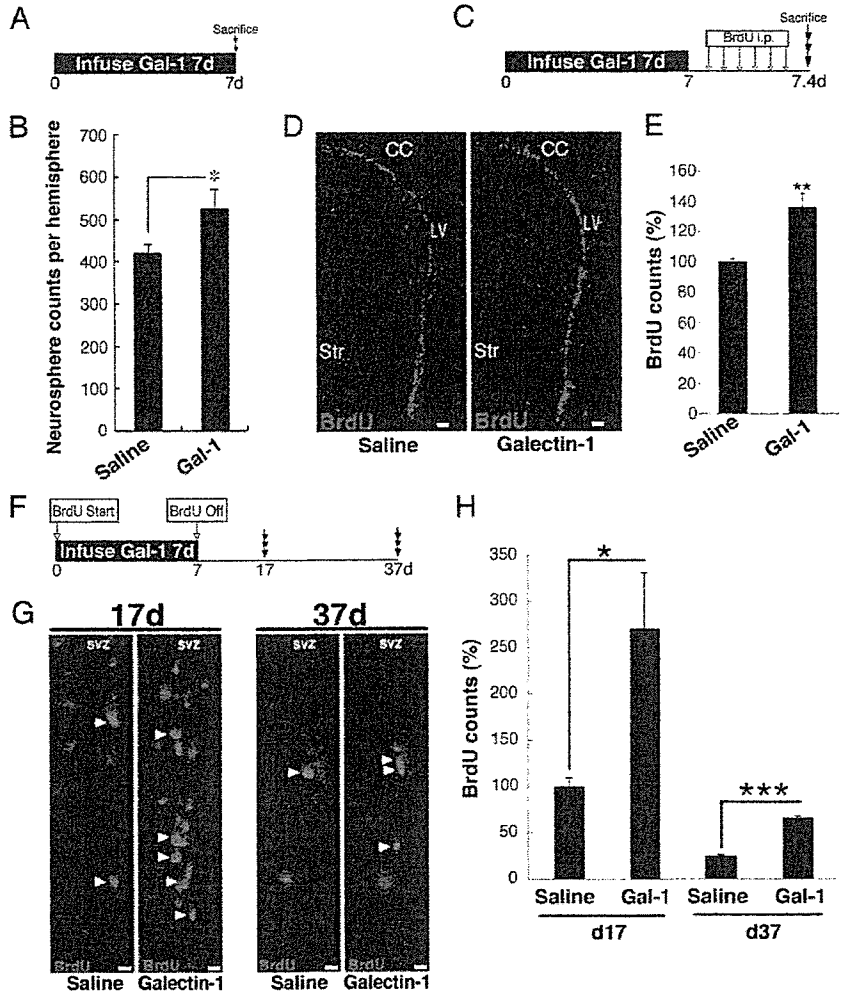

Fig. 3. Galectin-1 facilitates neural progenitor cell proliferation in the adult FB. (*A*) Experimental schema of the neurosphere formation assay after Galectin-1 infusion. (*B*) Galectin-1 significantly increased the number of neurosphere-initiating cells in the SVZ. *, $P < 0.05$. (*C*) Experimental schema of BrdU infusion after Galectin-1 infusion. (*D*) Low-magnification images of BrdU$^+$ cells in the SVZ after Galectin-1 infusion. (*E*) Galectin-1 infusion significantly increased the number of BrdU$^+$ cells in the SVZ. **, $P < 0.01$. (*F*) Experimental schema for labeling cells that retained BrdU long after Galectin-1 infusion. The mice were killed at the 17- or 37-day time point. (*G*) BrdU-labeled cells after infusion of saline or Galectin-1. (*H*) In the Galectin-1-infused brain, the number of BrdU$^+$ cells was significantly greater than in the saline-treated brain at 17 and 37 days. *, $P = 0.01$; ***, $P = 0.0006$. Str, striatum. (Scale bars: *D*, 50 μm; *G*, 15 μm.)

anti-Galectin-1 and anti-GFAP Abs to determine the percentages of each cell population in the SVZ. Of the total SVZ cells counted (n = 336 from three mice), 32.7 ± 6.38% (110 cells) were Galectin-1$^+$, and 31.3 ± 6.99% (105 cells) were GFAP$^+$. Of the GFAP$^+$ cells, 71.4 ± 1.48% were also Galectin-1$^+$. These results suggest that Galectin-1 is expressed in a subset of SVZ astrocytes.

To detect the slowly dividing NSC population in the SVZ (37), we gave BrdU to mice in their drinking water for 2 weeks and killed the mice 10 days later (Fig. 2*B*); this delay allowed the BrdU in the rapidly dividing type C cell population to be washed out and the type A cell population to migrate to a more rostral region, out of the SVZ (37). A subpopulation of the long-term BrdU-retaining cells expressed Galectin-1 (Fig. 2*C*). Thus, we conclude that Galectin-1 is expressed in a subset of GFAP$^+$ SVZ astrocytes that includes NSCs.

Galectin-1 Facilitates Proliferation of Neural Progenitor Cells in the Adult FB. The *in vitro* functions and *in vivo* expression pattern of Galectin-1 led us to examine whether it promotes adult neural progenitor proliferation *in vivo*. Galectin-1 protein was infused into the mouse LV for 7 days, and the number of neurospheres derived from the SVZ was counted (Fig. 3*A*); this number should reflect the number of progenitor cell types in the SVZ, including type B and C cells (36). As expected, significantly more neurospheres were formed by SVZ cells from the Galectin-1-infused adult brains than by SVZ cells from the control brains (Fig. 3*B*). The neurospheres in these cultures retained the properties of stem cells *in vitro*, and the proportion of neurons produced from the spheres was not significantly different (Galectin-1, 7.61 ± 0.61%; control, 5.84 ± 0.47%).

Next, we tested the effects of Galectin-1 on cell proliferation in the SVZ by infusing it into the LV, followed by BrdU injections every 2 h for 10 h (Fig. 3*C*). Thirty minutes after the last BrdU injection, the mice were killed. We counted the number of BrdU$^+$ cells in the SVZ of the LV and found a significant increase, on average, compared with the saline-infused control group (Fig. 3 *D* and *E*; $P < 0.01$; $n > 3$ mice each). There was no significant difference in the number of apoptotic cells in the SVZ between the two groups (Fig. 9 *A* and *B*, which is published as supporting information on the PNAS web site), suggesting that the Galectin-1-induced increase in BrdU$^+$ cells was caused by increased proliferation rather than increased cell survival.

Table 1. Galectin-1 increases the number of SVZ astrocytes in the adult brain

Treatment	No. of cells		
	Type B	Type C	Type A
Saline	40 ± 14	200 ± 12	64 ± 6.6
Galectin-1	66 ± 7.0*	280 ± 2.0*	64 ± 31
Galectin-1/saline relative ratio	1.7	1.4	1.0

Significantly increased numbers of SVZ astrocytes (type B cells) and type C cells were observed in the Galectin-1-infused brain. Data are the average counts from 50-μm sections. *, $P < 0.05$.

To determine what type of cells in the SVZ proliferated in response to the Galectin-1 infusion, we used cell-type markers (Fig. 10, which is published as supporting information on the PNAS web site) that allowed us to distinguish proliferating type B ($BrdU^+/Sox21^+/Dlx^-$), type C ($BrdU^+/Mash1^+$), and type A ($BrdU^+/Dlx^+/Mash1^-$) cells from others ($BrdU^+/Sox21^-$) (Table 1; see *Materials and Methods* for details). The Galectin-1 infusion significantly increased the number of proliferating type B and C cells (Table 1; $P < 0.05$, Mann–Whitney U test).

Infusion of Galectin-1 Protein Increases the Slowly Dividing SVZ Cells. We next examined the effect of Galectin-1 on the number of slowly dividing cells. We gave BrdU to mice in their drinking water during the 1-week infusion of Galectin-1 protein and killed them 17 or 37 days after the beginning of the infusion (Fig. 3*F*). There were significantly more $BrdU^+$ cells in the SVZ of the Galectin-1-infused brains than in that of the control brains at both time points (Fig. 3 *G* and *H*; day 17, $P = 0.01$, $n > 3$ each; day 37, $P < 0.001$, $n > 3$ each). These data suggest that Galectin-1 infusion increased the population of slowly dividing SVZ progenitor cells.

Galectin-1 exists in either a reduced or oxidized form, and only the reduced form possesses carbohydrate-binding activity (38). The infusion of CS-Galectin-1, a reduced form in which all of the cysteines responsible for its oxidation have been converted to serine (39), significantly increased the number of slowly dividing cells (Fig. 11, which is published as supporting information on the PNAS web site; day 17, $P < 0.001$, $n > 5$ mice each). In contrast, the oxidized Galectin-1 did not have a significant effect (Fig. 11*C*). These results suggest that the carbohydrate-binding capacity of the extracellularly administrated Galectin-1 is required for its effect on the number of slowly dividing cells. We also found that CS-Galectin-1 could bind to SVZ cells, including $GFAP^+$ astrocytes (unpublished data), suggesting that these cells are responsive to Galectin-1.

***Galectin-1*-Null Mice Have Fewer Neural Progenitor Cells in the Adult Brain.** To study the function of endogenous Galectin-1 in adult neural progenitor cells, we analyzed the phenotype of adult *galectin-1* mutant mice. First, we counted the number of cycling cells in the SVZ by using proliferating cell nuclear antigen (PCNA), a proliferation marker (40), and found significantly fewer in the *galectin-1*-null mice than in their wild-type littermates (Fig. 4 *A–C*; $P < 0.01$; $n > 3$ each). We also examined the number of type C cells by counting the $Mash1^+$ cells, of which there were also significantly fewer in the *galectin-1*-null mice than in wild-type littermates (Fig. 4 *D–F*; $P < 0.05$; $n > 3$ each). We then treated the animals with BrdU for 2 weeks, followed by a 10-day wash-out period (Fig. 4*G*), and found that there were significantly fewer slowly dividing cells in the SVZ of the *galectin-1*-null mice than in their wild-type littermates (Fig. 4 *H–J*; $P < 0.01$; $n > 3$ each). Furthermore, infusion of an

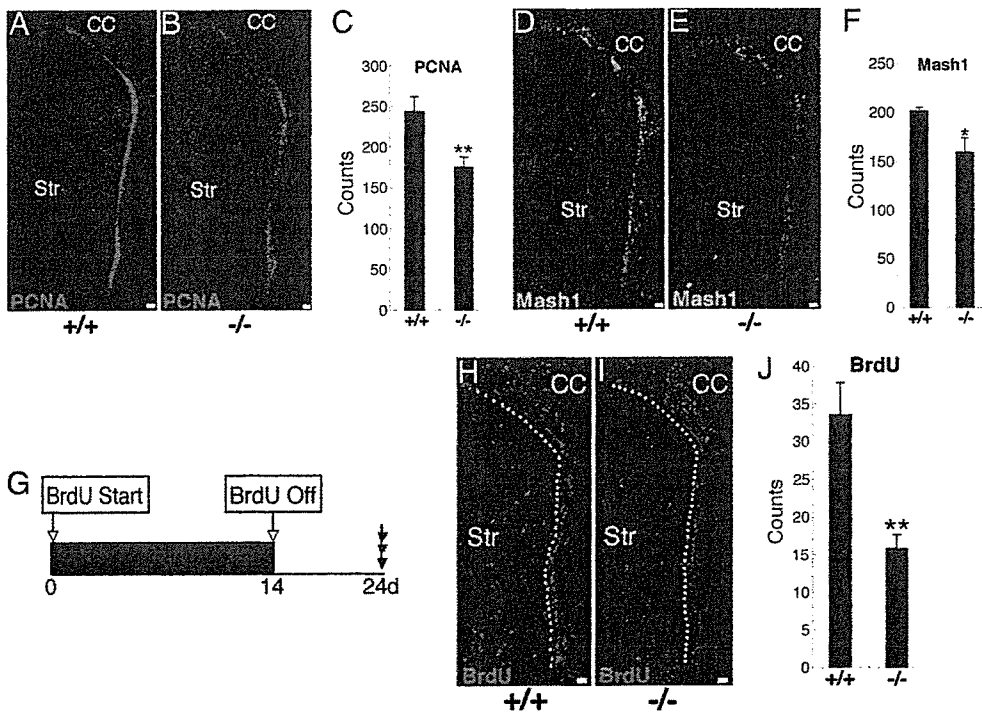

Fig. 4. Adult *galectin-1*-null mice show decreased neural progenitor cells. (*A–C*) Significantly fewer $PCNA^+$ cells were seen in the SVZ of *galectin-1*-null mice than in wild-type littermates. **, $P < 0.01$; $n > 3$ each. (*D–F*) Significantly fewer $Mash1^+$ type C cells were seen in the SVZ of *galectin-1* null mice than in wild-type littermates. *, $P < 0.05$; $n > 3$ each. (*G–J*) Fewer slowly dividing cells were seen in *galectin-1*-null mice than in wild-type mice. Slowly dividing cells in the SVZ were visualized as described in the legend of Fig. 2*B*. Dotted lines are drawn around the SVZ in *H* and *I*. (*J*) Significantly fewer long-term BrdU-retaining cells were observed in the SVZ of *galectin-1* mutant mice than in wild-type littermates. **, $P < 0.01$; $n > 3$ each. (Scale bars: 50 μm.)

anti-Galectin-1 neutralizing Ab (29) into the LV of adult wild-type mice significantly decreased the number of slowly dividing cells (Fig. 12, which is published as supporting information on the PNAS web site), a phenotype similar to that seen in *galectin-1*-null mutants (Fig. 4 *G–J*), suggesting that the endogenous Galectin-1 protein in the adult SVZ plays a role in the maintenance of neural progenitor cells. Moreover, the *galectin-1*-null mutation did not affect the number of apoptotic cells in the SVZ (Fig. 9 *C* and *D*). Together, these data suggest that Galectin-1 is required for the normal proliferation of type B and C cells in the adult brain.

The proliferation of adult and fetal NSCs is regulated by distinct mechanisms (41). Radial glial cells act as NSCs in the fetal and early postnatal brain and then may differentiate into astrocytes, expressing GFAP at approximately postnatal day (P) 7–15 (42, 43). Interestingly, Galectin-1 is not expressed before P9 in the FB (44). The brain of *galectin-1*-null mice at birth is indistinguishable from that of wild-type littermates (30, 45) except for an aberrant topography of olfactory axons (46). Therefore, Galectin-1 is most likely to play a role in adult NSCs rather than in embryonic NSCs. Taken together, our results demonstrate that Galectin-1 is expressed in slowly dividing SVZ astrocytes, which include the NSCs (34), and plays an important role in the proliferation of adult neural progenitor cells, including SVZ astrocytes. Stem cells reside in an area called a niche (47, 48), which has a characteristic cellular composition and signal mediators. In the niche, the state of each cell [i.e., cell cycle, apoptosis, and cell–cell or cell–extra cellular matrix (ECM) interactions] is strictly regulated to maintain stem cell homeostasis. Although ECM proteins are enriched in the SVZ (24, 49, 50), the niche for NSCs, the physiological significance of their carbohydrate structures has not been well characterized. In general, lectins exert their biological effects by binding to certain carbohydrate structures. Galectin-1's carbohydrate-binding ability is required for some functions but not others (27, 39, 51, 52). The present study suggests that the carbohydrate-binding activity of Galectin-1 is required for its promotion of adult neural progenitor cell proliferation. The analysis of Galectin-1 function will help us understand the important roles of carbohydrate molecules in stem cell biology, which may lead to the development of innovative therapies for human diseases.

Materials and Methods

Evaluation of OP9CM Activity. To assay the CM activity (see *Supporting Materials and Methods*, which is published as supporting information on the PNAS web site), neurospheres, prepared as described in ref. 53, were dissociated with trypsin and then FACS-sorted (*Supporting Materials and Methods*) at one cell per well directly into 96-well low-adhesion microtiter plates (Costar) containing each CM in a separate well. Human Galectin-1 was purchased from Genzyme Techne. To prepare the neurosphere CM (NSCM), neurospheres were cultured in the basal medium with 20 ng/ml human recombinant EGF (PeproTech, Rocky Hill, NJ) and FGF-2 (Genzyme Techne) for 48 h. To evaluate the activity of Galectin-1, the cells were sorted at 100 cells per well into NSCM-containing medium.

Molecular Identification of Galectin-1 in the CM. The OP9CM and IA-OP9CM preparations were analyzed by using the ProteinChip system (Ciphergen Biosystems). To screen the differences in peak heights, chemical surface chips that were positively charged, negatively charged, hydrophobic, C4, and Zn were used in the range of 500–200,000 Da. The affinity of the protein for each chip was monitored by using wash buffers of several pH values. To purify the 14.6-kDa protein, 200 ml of the OP9CM was freeze-dried, and a condensed solution was run on a Q-100 column (General Electric). The fraction that was eluted with 200 mM NaCl was used for SDS/PAGE. The 14.6-kDa band was cut from the gel and used for amino acid sequencing by tandem mass spectrometry.

Infusion into the SVZ and Adult Neurosphere Culture. Galectin-1 (2 or 14 μg), anti-Galectin-1 neutralizing Ab (rabbit IgG, 30 μg/ml, Kirin Brewery), or control rabbit IgG (30 μg/ml, Kirin Brewery) was dissolved in 0.9% saline with 1 mg/ml mouse serum albumin (Sigma) and infused into the LV as described in ref. 54 by using an osmotic pump (Alzet, Palo Alto, CA) at 0.5 μl/h for the given number of days. Adult neurosphere cultures from the infused brain samples were prepared as described in ref. 54.

Immunohistochemistry. Brains were perfusion-fixed with 4% paraformaldehyde (PFA) and postfixed in the same fixative overnight, and 50-μm sections were cut on a vibratome. Differentiated neurospheres grown on coverslips were immersion-fixed in 4% PFA for 15 min at room temperature. After three rinses in PBS, the neurospheres or sections were incubated for 1 h in TNB blocking solution (Vector Laboratories), incubated with primary antibodies overnight, and incubated for 60 min at room temperature with biotinylated secondary antibodies (1:200) or Alexa Fluor-conjugated secondary antibodies (1:200; Molecular Probes), unless otherwise noted. Biotinylated antibodies were visualized by using the Vectastain Elite ABC kit and TSA (Vector Laboratories). Anti-Galectin-1-neutralizing Abs were prepared as described in ref. 39. Other primary antibodies used in this study are described in *Supporting Materials and Methods*.

BrdU Labeling. For short-term labeling, after the intraventricular infusion of Galectin-1 for 7 days, mice received i.p. injections of BrdU (120 mg/kg dissolved in 0.007% NaOH in phosphate buffer; Sigma) every 2 h for 10 h and were killed 0.5 h after the last injection. For long-term labeling, 1 mg/ml BrdU was given to mice in their drinking water for 2 weeks (or 1 week in experiments involving the infusion of Galectin-1 or Abs). Mice were killed 10 or 30 days after the last day of infusion, and the brains were processed for immunohistochemistry.

Quantification of Histological Results. To quantify each cell type, 20 coronal vibratome sections of the SVZ (50 μm thick) were obtained at the level of the caudate-putamen (1.0–0 mm rostral to the bregma) from each hemisphere. The sections were stained for three different markers with BrdU (Sox21/BrdU, Dlx/BrdU, or Mash1/BrdU). Single confocal images were taken as 1-μm optical sections (LSM-510; Zeiss) from each vibratome section. The $BrdU^+$ nuclei that were positive for each marker (Sox21, Dlx, or Mash1) were counted, and the total number of $BrdU^+$ cells was multiplied by the ratio of the cells of each type to $BrdU^+$ cells, yielding the numbers for each cell type as follows: type B cells = total number of $BrdU^+$ [$(Sox21^+/BrdU^+)$ − $(Dlx^+/BrdU^+)$], type C cells = total number of $BrdU^+$ $(Mash1^+/BrdU^+)$, and type A cells = total number of $BrdU^+$ [$(Dlx^+/BrdU^+)$ − $(Mash1^+/BrdU^+)$]. The average number of each cell type per 50-μm section throughout the LV is indicated in each figure. Apoptotic cells were detected by using an ApoTag kit (Intergen, Purchase, NY). We quantified the cells in the LV contralateral to the infused side, because exposure to the increased concentration of reagent in the LV could have an artifactual effect.

Animals. For the adult mouse study, 8-week-old male mice were killed by anesthetic overdose. *galectin-1* knockout mice (129SJ background) are described in ref. 30. The animals were maintained on a 12-h light/12-h dark cycle with unlimited access to food and water. All experiments on live animals were performed in accordance with Keio University guidelines and regulations.